9

Atom Optomechanics

Philipp Treutlein

University of Basel, Department of Physics,
Switzerland

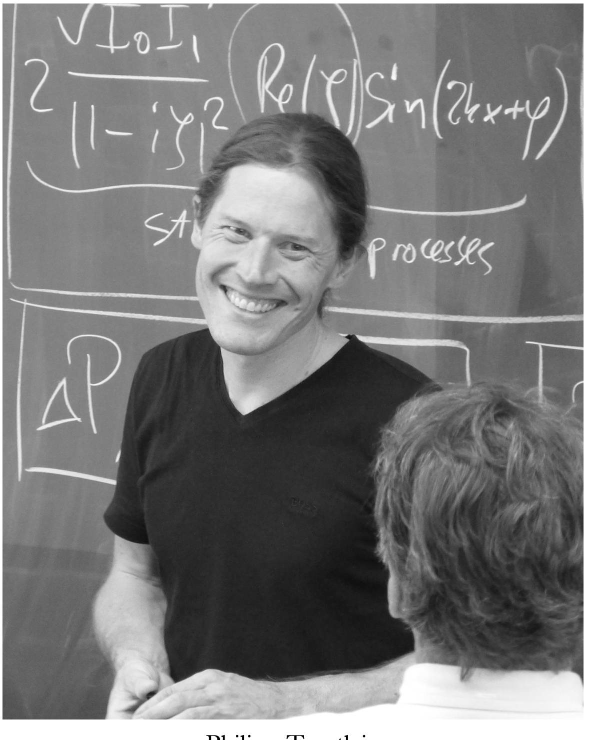

Philipp Treutlein

Philipp Treutlein, *Atom Optomechanics* In: *Quantum Optomechanics and Nanomechanics*. Edited by: Pierre-Francois Cohadon, Jack Harris, Florian Marquardt, Leticia F. Cugliandolo, Oxford University Press (2020).
DOI: 10.1093/oso/9780198828143.003.0009

Chapter Contents

These lecture notes give an introduction to optomechanics with ultracold atoms, focusing in particular on hybrid systems where atoms are interfaced with micro- and nanofabricated mechanical structures.

I would like to thank K. Hammerer, C. Genes, K. Stannigel, B. Vogell, M. Wallquist and P. Zoller for the fruitful collaborations which laid the theoretical ground for our atom-optomechanics activities. I am equally grateful to the talented and motivated students who have contributed to our experiments: D. Hunger, S. Camerer, M. Korppi, A. Jöckel, M. Mader, T. Lauber, M. T. Rakher, A. Faber, T. Kampschulte, L. Beguin, T. Karg and G. Buser. In particular, I would like to thank T. Karg for helping with the preparation of these lecture notes.

9.1 Introduction

The mechanical effects of light on matter are at the heart of research in the fields of optomechanics and ultracold atoms. In optomechanics, a growing community of researchers is developing techniques for laser cooling, manipulation, and measurement of micro- and nanofabricated mechanical oscillators (Aspelmeyer *et al.*, 2012; Aspelmeyer *et al.*, 2014). An important goal is to control mechanical vibrations of a massive solid-state oscillator on the quantum level and to exploit this control for fundamental tests of quantum physics and applications in precision sensing and signal transduction.

For ultracold atoms, quantum control of mechanical vibrations is well established. The techniques of laser cooling and trapping developed since the 1980s allow one to prepare single atoms as well as large ensembles in the ground-state of a trap, to coherently manipulate their motion, and to detect their vibrations with quantum-limited precision (Chu, 1991; Adams and Riis, 1997; Chu, 2002; Weidemüller and Zimmermann, 2009). The coupling of ultracold atoms to the light field inside high-finesse cavities has been studied on the single-photon level in cavity quantum electrodynamics (Miller *et al.*, 2005; Tanji-Suzuki *et al.*, 2011). The availability of these techniques makes ultracold atoms attractive for optomechanics experiments deep in the quantum regime.

Atomic implementations of optomechanics give access to new regimes of optomechanical coupling, such as the 'granular' regime where the coupling of photons and phonons is significant at the level of single quanta (Stamper-Kurn, 2014), and connect optomechanics to research in many-body physics (Ritsch *et al.*, 2013). Besides their mechanical degrees of freedom, atoms have discrete internal levels that can be controlled with high fidelity. This adds new features to optomechanical systems such as two-level systems or collective spins that can be prepared in highly nonclassical states (Riedel *et al.*, 2010; Gross *et al.*, 2010; Vasilakis *et al.*, 2015; McConnell *et al.*, 2015). The new regimes and new functionality provided by atomic optomechanical systems are currently being explored in a number of experiments (Brennecke *et al.*, 2008; Murch *et al.*, 2008; Purdy *et al.*, 2010; Schleier-Smith *et al.*, 2011; Wolke *et al.*, 2012).

The close analogies between optomechanics and laser manipulation of atoms have also played a role in the development of hybrid mechanical-atomic systems (Hunger *et al.*, 2011; Treutlein *et al.*, 2014). In these systems, laser light is used to couple the vibrations of a solid-state mechanical oscillator to the vibrations or internal states of atoms in a trap. Hybrid mechanical-atomic systems provide new opportunities for quantum control. For example, atoms can enhance the optomechanical cooling of mechanical oscillators, which could enable ground-state cooling in regimes where purely optomechanical techniques fail (Genes *et al.*, 2011; Vogell *et al.*, 2013; Bennett *et al.*, 2014; Bariani *et al.*, 2014). By engineering strong coherent interactions between mechanical oscillator and atoms, non-classical atomic states could be swapped to the mechanical device, realizing non-classical states of mechanical motion (Hammerer *et al.*, 2009*b*; Vogell *et al.*, 2015). Coupling a mechanical oscillator to a spin oscillator with negative effective mass allows one to create Einstein–Podolsky–Rosen entanglement between the two systems, which could be exploited for remote sensing of mechanical vibrations with a precision beyond the standard quantum limit (Hammerer *et al.*, 2009*a*; Polzik and Hammerer, 2015). Exploiting the nonlinearities offered by interacting atomic systems, control of mechanical vibrations on the level of single phonons could be achieved (Carmele *et al.*, 2014). The rich toolbox for quantum control and measurement of atoms thus becomes available for control of solid-state mechanical devices.

These lecture notes give an introduction to optomechanics with ultracold atoms, with a particular focus on hybrid systems. In the first half, we derive the basic optomechanical interactions of atoms and light. Section 9.2 introduces essentials of atom trapping in far-detuned laser light. In section 9.3 we discuss the properties of trapped atoms as mechanical oscillators from an optomechanics point of view. Section 9.4 presents a very useful model to describe the optomechanical interactions of atoms and light, treating the atoms as polarizable particles. In section 9.5, we use this model to derive the optomechanical coupling of atoms and a cavity field and briefly review cavity optomechanics experiments with atoms in the quantum regime.

The second half of the chapter is devoted to hybrid mechanical-atomic systems. We start with an overview of different coupling mechanisms that are explored in recent experiments (section 9.6). In the following, we focus on light-mediated interactions and derive the long-distance coupling of a membrane to an ensemble of laser-cooled atoms (section 9.7). In section 9.8 we review experiments on sympathetic cooling of a membrane with cold atoms. The requirements and perspectives for mechanical quantum control are discussed in section 9.9. In section 9.10 we introduce the new possibilities that arise if the mechanical oscillator is coupled to the atomic internal state.

9.2 Optical Forces on Atoms

Laser light can exert forces on matter through radiation pressure. Harnessing these forces for laser cooling and trapping of atoms triggered a revolution in the field of atomic physics, which led to the observation of new quantum states of matter such as Bose–Einstein condensates, first implementations of quantum information processing tasks, and the development of precision measurement devices such as atomic fountain clocks and atom interferometers (Chu, 1991; Adams and Riis, 1997; Chu, 2002; Weidemüller and Zimmermann, 2009). One distinguishes two types of optical forces on atoms:

- The *optical dipole force* arises from absorption of photons by the atom followed by stimulated reemission into the laser field. This is a coherent process that results in a redistribution of photons between laser field modes and an associated momentum transfer to the atom. The optical dipole force is conservative and it is frequently used for atom trapping, but it also plays a role in sub-Doppler laser cooling.
- The *scattering force* has its origin in absorption of photons followed by spontaneous emission. This is an incoherent process whereby photons are taken from the incident laser field and scattered into vacuum field modes. The scattering force is dissipative and it is mostly used in laser cooling.

We will discuss basic properties of these forces for the case of an atom with an optical transition at frequency ω_0 and natural linewidth $\Gamma = 1/\tau$, where τ is the excited-state lifetime. As an example, consider the D2 line of ^{87}Rb with $\omega_0 = 2\pi \times 384$ THz, corresponding to a wavelength of 780 nm, and $\Gamma = 2\pi \times 6$ MHz. We focus on the experimentally relevant case where the driving laser field at frequency ω is far-detuned from the atomic transition, so that the detuning $\Delta = \omega - \omega_0$ satisfies $|\Delta| \gg \Gamma$ and the atomic transition is very far from being saturated. In this regime, the optical dipole force is much stronger than the scattering force, as we will see below. A very useful review of far-detuned optical dipole traps is given in (Grimm *et al.*, 2000), which forms the basis of the following discussion.

9.2.1 Optical Dipole Force and Photon Scattering Rate

We consider an atom driven by a classical laser field

$$\mathbf{E}(\mathbf{r},t) = \tfrac{1}{2}\,\mathbf{e}\,\tilde{E}(\mathbf{r})\,e^{-i\omega t} + \text{c.c.} \tag{9.1}$$

The field induces an oscillating electric dipole moment in the atom,

$$\mathbf{p}(\mathbf{r},t) = \tfrac{1}{2}\,\mathbf{e}\,\tilde{p}(\mathbf{r})\,e^{-i\omega t} + \text{c.c.} \tag{9.2}$$

with $\tilde{p} = \alpha\tilde{E}$, where $\alpha = \alpha(\omega)$ is the frequency-dependent, complex atomic polarizability. The interaction potential of this induced dipole in the driving laser field is

$$U_{\text{dip}}(\mathbf{r}) = -\frac{1}{2}\langle \mathbf{p}(\mathbf{r},t)\cdot\mathbf{E}(\mathbf{r},t)\rangle = -\frac{1}{2\epsilon_0 c}\text{Re}(\alpha)I(\mathbf{r}). \tag{9.3}$$

Here, $\langle\cdot\rangle$ denotes a time average over one oscillation period of the electric field and the electric field intensity is $I(\mathbf{r}) = \frac{1}{2}\epsilon_0 c|\tilde{E}(\mathbf{r})|^2$. The optical dipole force is given by the gradient of the potential

$$\mathbf{F}_{\text{dip}}(\mathbf{r}) = -\nabla U_{\text{dip}}(\mathbf{r}) = \frac{1}{2\epsilon_0 c}\Re(\alpha)\nabla I(\mathbf{r}). \tag{9.4}$$

The dipole force is a conservative force that depends on the real part $\Re(\alpha)$ of the atomic polarizability, representing the in-phase response of the atom.

The power absorbed by the oscillator from the driving field and re-emitted as dipole radiation into free space is given by

$$P_{\text{abs}} = \langle \dot{\mathbf{p}} \cdot \mathbf{E} \rangle = \frac{\omega}{\epsilon_0 c} \Im(\alpha) I. \tag{9.5}$$

It depends on the imaginary part $\Im(\alpha)$ of the atomic polarizability, representing the out-of-phase response of the atom. In a photon picture, the underlying process is absorption of photons followed by spontaneous emission. The corresponding photon scattering rate is

$$\Gamma_{\text{sc}}(\mathbf{r}) = \frac{P_{\text{abs}}}{\hbar\omega} = \frac{1}{\hbar\epsilon_0 c} \Im(\alpha) I(\mathbf{r}). \tag{9.6}$$

The above expressions for the optical dipole potential and the photon scattering rate hold for any polarizable neutral particle in an oscillating electric field, as long as a proper model for the polarizability α is used. For example, they also apply to experiments with levitated dielectric nanoparticles (Romero-Isart *et al.*, 2011).

9.2.2 Oscillator Model and Atomic Polarizability

There are different ways to describe the atom–light interaction and to derive the optical forces on an atom. If the atomic transition is far from being saturated, we can use the Lorentz oscillator model of the atom to obtain the atomic polarizability. In section 9.2.4, we will briefly discuss the connections to the two-level model.

In the Lorentz model, an electron of charge $-e$ and mass m_e is considered to be elastically bound to the atomic core, forming a simple harmonic oscillator of eigenfrequency ω_0. The oscillator is damped at a rate Γ_ω due to the power radiated by the accelerated charge. The equation of motion of the oscillator driven by the electric field is thus

$$\frac{d^2x}{dt^2} + \Gamma_\omega \frac{dx}{dt} + \omega_0^2 x = -\frac{e}{m_e} E(t), \tag{9.7}$$

where x is the distance of the electron from the core. Transforming this equation to the frequency domain $[x(t) = \frac{1}{2}\tilde{x}e^{-i\omega t} + \text{c.c.}]$ yields

$$-\omega^2 \tilde{x} - i\omega\Gamma_\omega \tilde{x} + \omega_0^2 \tilde{x} = -\frac{e}{m_e} \tilde{E}. \tag{9.8}$$

The induced electric dipole moment of the atom is $\tilde{p} = -e\tilde{x}$. Using Eq. (9.8) and $\tilde{p} = \alpha\tilde{E}$ we obtain the complex atomic polarizability

$$\alpha(\omega) = \frac{e^2}{m_e} \cdot \frac{1}{\omega_0^2 - \omega^2 - i\omega\Gamma_\omega}. \tag{9.9}$$

The classical damping rate of an oscillating charge due to radiative energy loss is given by (Feynman *et al.*, 1964)

$$\Gamma_\omega = \frac{e^2\omega^2}{6\pi\epsilon_0 m_e c^3}. \tag{9.10}$$

Using Eq. (9.10) and $\Gamma \equiv \Gamma_{\omega_0} = \frac{\omega_0^2}{\omega^2}\Gamma_\omega$ we can rewrite the atomic polarizability as

$$\alpha(\omega) = \frac{6\pi\epsilon_0 c^3}{\omega_0^2} \cdot \frac{\Gamma}{\omega_0^2 - \omega^2 - i(\omega^3/\omega_0^2)\Gamma}. \tag{9.11}$$

For detunings $|\Delta| \ll \omega_0$ we can approximate $\omega_0^2 - \omega^2 \approx -2\omega_0\Delta$ and $\omega/\omega_0 \approx 1$. Within this rotating-wave approximation the atomic polarizability is

$$\alpha \simeq -\frac{3\pi\epsilon_0 c^3}{\omega_0^3} \cdot \frac{\Gamma}{\Delta + i\Gamma/2} = -\frac{3\pi\epsilon_0 c^3}{\omega_0^3} \cdot \frac{\Gamma}{\Delta} \cdot \frac{1 - i\frac{\Gamma}{2\Delta}}{1 + \left(\frac{\Gamma}{2\Delta}\right)^2}. \tag{9.12}$$

For $|\Delta| \gg \Gamma$ we can expand to second order in Γ/Δ and find

$$\alpha \simeq -\frac{3\pi\epsilon_0 c^3}{\omega_0^3} \cdot \frac{\Gamma}{\Delta} \cdot \left(1 - i\frac{\Gamma}{2\Delta}\right), \tag{9.13}$$

which is the atomic polarizability for far-detuned radiation and a single optical transition without substructure.

Inserting this result in Eqs. (9.3) and (9.6), we obtain the optical dipole potential and scattering rate for far-detuned radiation:

$$U_{\text{dip}}(\mathbf{r}) \simeq \frac{3\pi c^2}{2\omega_0^3} \cdot \frac{\Gamma}{\Delta} \cdot I(\mathbf{r}), \tag{9.14}$$

$$\Gamma_{\text{sc}}(\mathbf{r}) \simeq \frac{3\pi c^2}{2\hbar\omega_0^3} \cdot \left(\frac{\Gamma}{\Delta}\right)^2 \cdot I(\mathbf{r}). \tag{9.15}$$

The two quantities are related by

$$\hbar\Gamma_{\text{sc}} = \frac{\Gamma}{\Delta} U_{\text{dip}}, \tag{9.16}$$

a consequence of the relation between the dispersive and absorptive properties of the atom. From Eq. (9.14) we can read off the important property that the sign of the dipole potential depends on the sign of the detuning of the laser from the atomic resonance:

red detuning	$(\Delta < 0)$	$\Rightarrow$	attractive potential
blue detuning	$(\Delta > 0)$	$\Rightarrow$	repulsive potential

Moreover, since $U_{\mathrm{dip}} \sim I/\Delta$ but $\Gamma_{\mathrm{sc}} \sim I/\Delta^2$, one can make the scattering rate negligible by working at large detuning and high laser power. The resonant character of the atom–light interaction and the tunability it offers are one of the main differences between atom trapping and levitation of dielectric nanoparticles.

So far we have neglected the fine and hyperfine structure of the atom. For alkali atoms, Eq. (9.13) correctly describes the case where Δ is much larger than the fine structure splitting of the D1 and D2 lines. For detunings such that the fine structure is resolved, the two lines have to be treated separately. If the detuning is still much larger than the hyperfine splitting and the laser is linearly polarized, α takes the form Eq. (9.13) multiplied by the line strength factor 1/3 (2/3) for D1 (D2). For general laser polarization or a detuning that resolves the hyperfine structure, α depends on the ground-state hyperfine level in which the atom is prepared. Formulae for various relevant cases are given in (Grimm *et al.*, 2000).

9.2.3 Scattering Force

The scattering force on an atom is due to absorption of photons followed by spontaneous emission. It is thus connected to the scattering rate Γ_{sc}. Every absorption event goes along with a momentum kick $\hbar\mathbf{k}$ on the atom, where $\mathbf{k}$ is the wave vector of the laser mode from which the photons is absorbed. When the photon is spontaneously reemitted into the vacuum field mode $\mathbf{k}'$, the atom received another momentum kick of $-\hbar\mathbf{k}'$. Since spontaneous emission is a random process that occurs with equal probability into opposite directions, the mean momentum transfer due to the emission averages to zero over many absorption–emission cycles. Therefore, only the absorption processes contribute to the mean scattering force. For a single laser mode of wave vector $\mathbf{k}$, the mean scattering force is

$$\mathbf{F}_{\mathrm{sc}} = \hbar\mathbf{k}\,\Gamma_{\mathrm{sc}}. \tag{9.17}$$

Compare this to the dipole force $\mathbf{F}_{\mathrm{dip}} = -\nabla U_{\mathrm{dip}}$. For a tightly focused laser beam or a standing wave of light, the intensity and thus the dipole potential varies on the wavelength scale, $\nabla U_{\mathrm{dip}} \approx kU_{\mathrm{dip}}$. Using this and Eq. (9.16), we can estimate

$$\frac{F_{\mathrm{sc}}}{F_{\mathrm{dip}}} \sim \frac{\hbar k\Gamma_{\mathrm{sc}}}{kU_{\mathrm{dip}}} = \frac{\Gamma}{\Delta}. \tag{9.18}$$

While the scattering force is important for near-resonant light such as in laser cooling of atoms, it is much weaker than the optical dipole force in far-detuned optical traps with $|\Delta| \gg \Gamma$.

9.2.4 Two-level model of the atom

The results of the previous sections can also be obtained in a two-level model of the atom. In the electric dipole approximation, the atom–light interaction Hamiltonian is

$$\hat{V}(\mathbf{r}) = -\hat{\boldsymbol{\mu}} \cdot \mathbf{E}(\mathbf{r}), \tag{9.19}$$

where $\hat{\boldsymbol{\mu}} = -e\hat{\mathbf{x}}$ is the electric dipole operator and $\hat{\mathbf{x}}$ refers to the position of the electron in the atom.

In the limit of large detuning $|\Delta| \gg (\Gamma, |\Omega_R|)$ one can apply second-order perturbation theory to calculate the energy shift of the atomic ground state $|g\rangle$ due to the atom–light interaction (also called 'light shift' or 'AC Stark shift'):

$$U_{\text{dip}}(\mathbf{r}) = \frac{\left|\langle e|\hat{V}(\mathbf{r})|g\rangle\right|^2}{\hbar\Delta} = \frac{\hbar|\Omega_R(\mathbf{r})|^2}{4\Delta}. \tag{9.20}$$

Here, $\Omega_R = \frac{1}{\hbar}\langle e|\hat{\boldsymbol{\mu}}|g\rangle \cdot \tilde{\mathbf{E}}(\mathbf{r})$ is the Rabi frequency of the driving laser on the optical transition of the atom.

The atomic excited state radiatively decays at a rate Γ. In steady state, the excited state population of the laser-driven atom is $\frac{|\Omega_R|^2}{4\Delta^2}$. Hence the photon scattering rate is given by

$$\Gamma_{\text{sc}} = \Gamma \, \frac{|\Omega_R|^2}{4\Delta^2}. \tag{9.21}$$

According to the Wigner–Weisskopf theory, the spontaneous decay rate is related to the dipole matrix element as

$$\Gamma = \frac{\omega_0^3}{3\pi\epsilon_0\hbar c^3}\left|\langle e|\hat{\boldsymbol{\mu}}|g\rangle\right|^2. \tag{9.22}$$

This allows us to express the Rabi frequency as

$$|\Omega_R|^2 = \Gamma \, \frac{3\pi\epsilon_0 c^3}{\hbar\omega_0^3}\,|\tilde{E}|^2 = \Gamma \, \frac{6\pi c^2}{\hbar\omega_0^3}\, I \tag{9.23}$$

Inserting this expression in Eqs. (9.20) and (9.21) reproduces the expressions for the dipole potential Eq. (9.14) and scattering rate Eq. (9.15) obtained from the Lorentz oscillator model in the far-detuned limit.

9.3 Trapped Atoms as Mechanical Oscillators

An atom trapped in a far-detuned optical trap is a microscopic mechanical oscillator that can be prepared and manipulated deep in the quantum regime using the well-established techniques of atomic physics. A trapped ensemble of N atoms represents a collection of mechanical oscillators with similar frequency. The centre-of-mass mode of the ensemble behaves like a simple harmonic oscillator with the same frequency as a single atom but N times larger mass. In this chapter, we will discuss the properties of such atomic mechanical oscillators.

9.3.1 One-dimensional Optical Lattice

For concreteness, we consider an atom in a one-dimensional optical lattice potential (Bloch, 2005), see Fig. 9.1. The lattice is generated by interference of two counterpropagating laser beams of equal intensity I_0, wave vector k, and detuning Δ from atomic resonance. The resulting standing-wave intensity pattern is

$$I(x) = 4I_0 \cos^2(kx), \tag{9.24}$$

where I_0 is the single-beam intensity. The far-detuned optical dipole potential obtained from Eq. (9.14) is

$$U_{\text{dip}} = V_m \cos^2(kx) \tag{9.25}$$

with a modulation depth

$$V_m = \frac{3\pi c^2}{2\omega_0^3} \frac{\Gamma}{\Delta} 4I_0. \tag{9.26}$$

If the laser is red detuned, $\Delta < 0$, the potential is attractive and the atoms are trapped near the intensity maxima of the standing wave. Using standard techniques of laser cooling (see section 9.3.2), the atoms can be prepared with energies $\ll |V_m|$, so that they are confined near the bottom of the sinusoidal potential wells. In a harmonic approximation to the trap bottom ($kx \ll 1$),

$$U_{\text{dip}} \simeq V_m - V_m k^2 x^2 \stackrel{!}{=} V_m + \frac{1}{2} m\Omega_a^2 x^2, \tag{9.27}$$

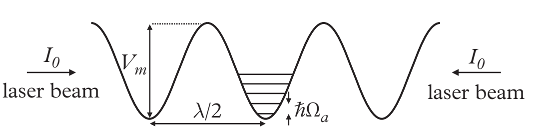

Fig. 9.1 *One-dimensional optical lattice potential created by interference of two laser beams.*

where m is the atomic mass and the trap frequency is defined as

$$\Omega_a = \sqrt{\frac{2|V_m|k^2}{m}}. \tag{9.28}$$

An ultracold atom trapped in the lattice represents a mechanical oscillator whose frequency can be adjusted via the laser intensity or the detuning, $\Omega_a \propto \sqrt{I_0/|\Delta|}$. This allows for fast *in situ* changes of Ω_a, e.g. to bring the atoms in resonance with other systems.

If an ensemble of N atoms is prepared in the lattice, each atom experiences an optical dipole potential. As long as the back-action of the atoms onto the light field is small (see section 9.4), each atom can be treated as an independent oscillator of frequency Ω_a. The centre-of-mass mode of the ensemble represents a mechanical oscillator with the same frequency Ω_a as a single atom, but the mass is increased to Nm. Deviations from this idealized picture arise e.g. from inhomogeneities across the ensemble due to the intensity profile of the trapping beams, which limit the mechanical quality factor of the centre-of-mass mode (see section 9.3.3).

In a red-detuned lattice ($\Delta < 0$), transverse confinement of the atoms is automatically provided by the transverse Gaussian laser profile. In the case of a blue-detuned lattice ($\Delta > 0$), the atoms are trapped near the intensity minima of the standing wave, but Eq. (9.28) for the lattice trap frequency still holds. In this case, the transverse confinement needs to be provided by another trapping beam. Conveniently, the beams creating the lattice usually need not be interferometrically stabilized. Fluctuations in the relative phase of the two beams only lead to a translation of the lattice potential but do not change its shape. Since these fluctuations usually are small and occur at frequencies far below Ω_a, the atoms can adiabatically follow the lattice position.

9.3.2 Ground-state Cooling of Atoms

With atoms in an optical lattice, mechanical frequencies up to a few MHz can be achieved (see also Table 9.1). To prepare the atoms in the ground state of the lattice potential, i.e. to reach $k_B T < \hbar\Omega_a$, microkelvin temperatures are required. Such low temperatures are routinely achieved using the techniques of atomic laser cooling (Adams and Riis, 1997). In the case of Rb atoms, simple optical molasses cooling provides temperatures $< 10\ \mu$K

Table 9.1 *Parameters of rubidium atoms trapped in a one-dimensional optical lattice. P is the single-beam power and S the beam cross-sectional area so that the peak intensity is $I_0 = P/S$.*

P	S	$\Delta/2\pi$	$\Omega_a/2\pi$	$x_{\mathrm{a,zpf}}$	Γ_{heat}
1 W	$(250\ \mu\mathrm{m})^2$	10^5 GHz	50 kHz	34 nm	5 mHz
1 mW	$(250\ \mu\mathrm{m})^2$	1 GHz	510 kHz	11 nm	5 kHz

in all three dimensions. Moreover, these cooling techniques have been shown to work well in the presence of optical lattice potentials (Winoto *et al.*, 1999). More advanced laser cooling techniques such as Raman sideband cooling (Kerman *et al.*, 2000; Treutlein *et al.*, 2001) have been used to achieve temperatures of a few hundred nanokelvin, preparing a large fraction of the atoms in the ground state of the lattice.

Since these laser cooling techniques cool each atom individually, all vibrational modes of an atomic ensemble are simultaneously cooled. Coupling between different vibrational modes of the ensemble, while providing a mechanism of mechanical decoherence, does not lead to heating because all modes are cold.

In ultracold atom experiments, the atoms are trapped under ultra-high vacuum conditions, with typical pressures in the range of 10^{-10} mbar and lower. Under these conditions, the atoms are very well isolated from the environment. The experimental apparatus itself is at room temperature, cryogenic cooling is not required. Decoherence of atomic motion mainly arises from the intrinsic fluctuations of the trapping potentials, which we discuss next.

9.3.3 Decoherence due to Photon Recoil Heating

So far, we have considered the mean optical forces experienced by the atom. They are the forces that remain in the limit of a classical polarizable object in a classical electromagnetic field. However, both the field as well as the induced atomic dipole show quantum fluctuations. These lead to fluctuations of the scattering force and the optical dipole force, which heat the trapped atoms and represent a fundamental source of decoherence in atom trapping.

In a red-detuned single-beam trap, the heating rate can be understood in terms of the spontaneous photon scattering at rate Γ_{sc} (Grimm *et al.*, 2000). Each scattered photon increases the energy of the atom by an amount proportional to the photon recoil energy $E_r = \hbar^2 k^2/2m$. In a standing-wave trap, as in Fig. 9.1, the situation is more subtle: both the spontaneous photon scattering as well as the quantum fluctuations of the dipole force contribute to the heating. The resulting heating power is (Gordon and Ashkin, 1980)

$$P_{\mathrm{heat}} = E_r \cdot \Gamma_{\mathrm{sc,max}} = E_r \frac{\Gamma V_m}{\hbar \Delta}, \tag{9.29}$$

where $\Gamma_{\mathrm{sc,max}}$ is the maximum photon scattering rate in the lattice, i.e. the rate evaluated at the intensity maxima. Note that P_{heat} is independent of the position in the lattice and independent of the sign of the detuning, so that blue- and red-detuned lattices show the same heating rate.

The resulting phonon heating rate along the lattice direction, Γ_{heat}, limits the coherent manipulation of the atomic motion. For example, the coherence time of the vibrational ground state is limited by $1/\Gamma_{\mathrm{heat}}$. Neglecting the three-dimensional character of the heating, we can estimate

$$\Gamma_{\text{heat}} = \frac{P_{\text{heat}}}{\hbar\Omega_a} = (kx_{\text{a,zpf}})^2\,\Gamma_{\text{sc,max}}. \tag{9.30}$$

Here, $x_{\text{a,zpf}} = \sqrt{\hbar/2m\Omega_a}$ is the atomic zero-point motion. Note that for typical parameters, $kx_{\text{a,zpf}} = \sqrt{E_r/\hbar\Omega_a} \ll 1$ and therefore $\Gamma_{\text{heat}} \ll \Gamma_{\text{sc,max}}$. This means that many photons need to be scattered to change the vibrational quantum state of the atom by one phonon.

Table 9.1 shows parameters for atomic mechanical oscillators in a one-dimensional optical lattice. The heating rate Γ_{heat} is usually smaller than the typical cooling rates of a few kHz achievable with atomic laser cooling techniques. The atoms can therefore be prepared in the ground-state of the lattice potential using standard laser cooling techniques as discussed in section 9.3.2. In very far-detuned lattices, the heating rate is so small that the atomic motion can be coherently manipulated on timescales of milliseconds or even seconds.

In experiments with micro- and nanofabricated mechanical oscillators, the mechanical quality factor is a key parameter that determines also the thermal heating rate. In the case of trapped atoms, the situation is very different. In contrast to nanomechanical oscillators, which are clamped to a support, trapped atoms in an ultra-high vacuum chamber are nearly perfectly isolated. The quality factor $Q_a = \Omega_a/\Gamma_a$, where Γ_a is the mechanical linewidth, is typically limited by trap anharmonicities, by drifts in the trapping potential, or, in the case of atomic ensembles, by inhomogeneities across the ensemble. These mechanisms result in pure dephasing or in a coupling of the mechanical mode of interest to other modes of the ensemble that are also at microkelvin temperatures. Although the resulting Q_a in the range of 10–10^4 is relatively small, there is negligible heating associated with these damping or dephasing mechanisms. When comparing with other systems, it is therefore more meaningful to compare the decoherence rates rather than the quality factors.

9.4 Atoms as Optical Elements

In the previous chapters, we treated the optical potential as a static container that holds the atoms and is not affected by their presence. This approximation is very well satisfied in most optical lattice experiments, where the lattice light is detuned by tens or even hundreds of nanometres from the atomic transition. In optomechanics experiments, on the other hand, the back-action of the atoms onto the light field is of primary interest. This implies that one needs to work at moderate detunings of the order of GHz. In this section, we discuss a model of atom–light interactions that is very well suited to describing optomechanics experiments with atoms (Asboth *et al.*, 2008). It treats the atoms as polarizable objects that are trapped by the light but also influence the propagation of the trapping fields in a consistent manner.

9.4.1 Beam-splitter Model of Atoms in an Optical Lattice

Consider a one-dimensional optical lattice whose transverse size is much larger than the $\lambda/2$ spacing of the lattice potential wells. Ultracold atoms tightly trapped in the lattice form an array of disc-shaped atomic clouds whose thickness is much smaller than λ. We can model the atoms in a given potential well as an infinitesimally thin sheet of polarizable material, containing N atoms of polarizability α in a cross-sectional area S, see Fig. 9.2. We consider for the moment just a single disc of atoms at position x_0 and model the incoming and outgoing light fields as plane waves with identical polarization and complex amplitudes E_i as shown in Fig. 9.2a.

To determine the light field in the presence of the atoms, we have to solve the scalar Helmholtz equation

$$\left(\partial_x^2 + k^2\right) E(x) = -2k\zeta E(x)\delta(x - x_0), \tag{9.31}$$

where the dimensionless coupling constant

$$\zeta = k \cdot \frac{N}{S} \cdot \frac{\alpha}{2\epsilon_0} \tag{9.32}$$

is proportional to the areal density of the cloud polarizability. Integrating Eq. (9.31) over a small interval centred at x_0, we obtain the boundary conditions for the electric field at the position of the atoms

$$\begin{aligned} E(x_0^-) &= E(x_0^+), \\ \partial_x E(x_0^-) &= \partial_x E(x_0^+) + 2k\zeta E(x_0). \end{aligned} \tag{9.33}$$

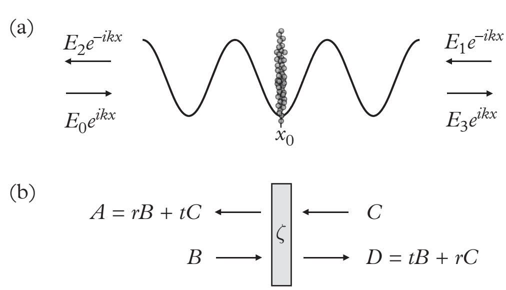

Fig. 9.2 *Atoms in one potential well of an optical lattice form a thin sheet of polarizable material that acts as a beam splitter for the light fields. (a) Incoming and outgoing electric fields modelled as plane waves with amplitudes E_i. (b) The atoms act as a beam splitter with reflection and transmission coefficients r and t, respectively. Here, $A = E_2e^{-ikx_0}$, $B = E_0e^{ikx_0}$, $C = E_1e^{-ikx_0}$, and $D = E_3e^{ikx_0}$ are the field amplitudes at the position of the atoms x_0.*

When evaluating these boundary conditions for the situation shown in Fig. 9.2a, it is useful to define the field amplitudes at the position of the atoms $A = E_2 e^{-ikx_0}$, $B = E_0 e^{ikx_0}$, $C = E_1 e^{-ikx_0}$, and $D = E_3 e^{ikx_0}$. We find that the thin sheet of atoms acts as a beam splitter with reflection and transmission coefficients

$$r = \frac{i\zeta}{1 - i\zeta}, \quad t = \frac{1}{1 - i\zeta}, \tag{9.34}$$

so that $\zeta = -ir/t$ and $A = rB + tC$ and $D = tB + rC$, see Fig. 9.2b.

These relations can also be expressed as a transfer matrix connecting the field amplitudes on the left of the atoms to those on the right,

$$\begin{pmatrix} A \\ B \end{pmatrix} = \begin{pmatrix} 1 + i\zeta & i\zeta \\ -i\zeta & 1 - i\zeta \end{pmatrix} \cdot \begin{pmatrix} C \\ D \end{pmatrix}. \tag{9.35}$$

Using the expression for α at large detuning from Eq. (9.13) we find

$$\zeta = -\frac{N\sigma}{2S} \cdot \frac{\Gamma}{2\Delta} \cdot \left(1 - i\frac{\Gamma}{2\Delta}\right), \tag{9.36}$$

where $\sigma = 3\lambda^2/(2\pi)$ is the resonant scattering cross-section of a single atom. The quantity $N\sigma/S$ is the resonant optical depth of the N atoms. This formalism now allows us to calculate the outgoing fields for given incoming fields and to determine the optical forces experienced by the atoms.

9.4.2 Optical Forces Experienced by the Atoms

The force F acting on the atomic cloud is determined by the rate at which momentum is extracted from the electromagnetic field. It can be expressed in terms of the power of the incoming and outgoing beams,

$$F = \frac{1}{c}\left(P_A + P_B - P_C - P_D\right), \tag{9.37}$$

reflecting the fact that a beam incident from the left (P_B) and being reflected to the left (P_A) results in a force to the right ($F > 0$), while a beam incident from the right (P_C) and being reflected to the right (P_D) leads to a force to the left ($F < 0$). Relating the power $P_A = I_A \cdot S$ to the intensity $I_A = \frac{1}{2}\epsilon_0 c|A|^2$ and similar for the other beams, we obtain

$$F = \frac{\epsilon_0}{2} \cdot S \cdot \left(|A|^2 + |B|^2 - |C|^2 - |D|^2\right). \tag{9.38}$$

The formalism described in the previous section allows us to express A and D in terms of the incoming fields $B = E_0 e^{ikx_0}$ and $C = E_1 e^{-ikx_0}$. Inserting the result in Eq. (9.38), we obtain the force as a function of the atomic position x_0 and the intensities of the incoming beams $I_0 \equiv I_B$ and $I_1 \equiv I_C$,

$$
\begin{aligned}
F(x_0) = {} & \left.\frac{2S}{c}(I_0 - I_1)\,\frac{\Im(\zeta)}{|1-i\zeta|^2}\right\} = F_{\mathrm{sc}} \\
& \left.-\frac{4S}{c}\sqrt{I_0 I_1}\,\frac{\Re(\zeta)}{|1-i\zeta|^2}\sin(2kx_0+\varphi)\right\} = F_{\mathrm{dip}} \\
& \left.+\frac{2S}{c}(I_0 - I_1)\,\frac{|\zeta|^2}{|1-i\zeta|^2}\right\} = F_{\mathrm{refl}}
\end{aligned}
\tag{9.39}
$$

where $\varphi = \arg(E_0) - \arg(E_1)$ is the relative phase of the two incoming beams at $x = 0$. The first term can be identified with the scattering force F_{sc} due to spontaneous scattering of photons out of the laser beams. The second term corresponds to the dipole force F_{dip} due to stimulated redistribution of photons between the two laser beams. The third term F_{refl} arises from the incoherent reflection of light at the atomic cloud. It is of order $|\zeta|^2$ and insensitive to the phase of the two incoming laser beams. Equation (9.39) allows us to calculate the optical force even in the regime $|\zeta| \gtrsim 1$ where the light field is strongly perturbed by the presence of the atoms.

The standard expressions for the optical dipole force and scattering force are obtained in the limit $|\zeta| \ll 1$, corresponding to low atomic density or small $|\alpha|$, where the back-action of the atoms on the light field is small. In this limit, the term F_{refl} is negligible and to lowest order in ζ we recover the results of section 9.2,

$$
\begin{aligned}
F(x_0) &\simeq \underbrace{\frac{2S}{c}\,(I_0 - I_1)\Im(\zeta)} - \underbrace{\frac{4S}{c}\sqrt{I_0 I_1}\,\Re(\zeta)\sin(2kx_0+\varphi)} \\
&= F_{\mathrm{sc}} + F_{\mathrm{dip}}.
\end{aligned}
\tag{9.40}
$$

If we furthermore take the limit of large detuning ($\Gamma/|\Delta| \ll 1$), only F_{dip} remains to lowest order.

9.4.3 Back-action of Atoms on the Light Field

The back-action of the atoms on the light field manifests itself in a modulation of the outgoing laser beams. For example, we find that the intensity I_A depends on the atomic position x_0,

$$
\begin{aligned}
I_A = {} & \left. I_1\,\frac{1}{|1-i\zeta|^2}\right\} \text{transmitted} \\
& \left. + I_0\,\frac{|\zeta|^2}{|1-i\zeta|^2}\right\} \text{incoherent reflection}
\end{aligned}
\tag{9.41}
$$

$$
\left.- 2\sqrt{I_0 I_1}\,\frac{\Re(\zeta)}{|1-i\zeta|^2}\sin(2kx_0+\varphi)\right\}\text{ stimulated processes}
$$

$$
\left.- 2\sqrt{I_0 I_1}\,\frac{\Im(\zeta)}{|1-i\zeta|^2}\cos(2kx_0+\varphi)\right\}\text{ scattering out of beam.}
$$

A similar expression holds for I_D, with I_0 and I_1 exchanged and opposite sign on the third line.

We can again take the limits $|\zeta| \ll 1$ and $\Gamma/|\Delta| \ll 1$ and find that the dominant terms are

$$
I_A \simeq I_1 - 2\sqrt{I_0 I_1}\,\Re(\zeta)\sin(2kx_0+\varphi) = I_1 + \frac{c}{2S}F_{\text{dip}}. \tag{9.42}
$$

Consequently, the transmitted beam is power modulated by $\delta P_A = \frac{c}{2}F_{\text{dip}}$, and similarly $\delta P_D = -\frac{c}{2}F_{\text{dip}}$. This back-action of the atoms onto the light field has been observed in a number of experiments (Kozuma *et al.*, 1996; Görlitz *et al.*, 1997; Raithel *et al.*, 1998). For large atom number and relatively near-resonant lattices, the power modulation can be quite substantial, on the order of a few percent.

9.4.4 Generalization to Multiple Clouds and Multi-level Atoms

So far we considered only a single disc of atoms in one well of the optical lattice potential. In general, many neighbouring wells will be filled with atoms. The transfer matrix formalism based on Eq. (9.35) is ideally suited to analyse this situation. In the regime $|\zeta| \gtrsim 1$ where the atoms strongly perturb the light field, new phenomena emerge which can be understood in terms of the light-mediated interactions between atoms in different potential wells (Asboth *et al.*, 2008). On the other hand, many experiments operate in the regime $|\zeta| \ll 1$. In this perturbative regime, the effects on the light field of atoms in different wells of the lattice simply add up, leading to the same results as if all atoms were placed in the same well.

Finally, we point out that the formalism described here has been generalized to the case of atoms with multiple internal states interacting with light fields of general polarization (Xuereb *et al.*, 2010). This allows one e.g. to describe polarization gradient laser cooling of atoms in counterpropagating laser beams. In the context of atom optomechanics experiments, it allows description of spin-optomechanics experiments where the atomic hyperfine spin state couples to the polarization state of the light field.

9.5 Cavity Optomechanics with Atoms

Ultracold atoms trapped in the light field of an optical cavity are a powerful and flexible system to study cavity optomechanics in the quantum regime. The optomechanical interaction of the atoms is analogous to that of thin dielectric membranes or levitated nanoparticles in optical cavities. We will make this analogy evident by describing the atoms as small polarizable objects using the formalism presented in section 9.4. Because the atoms are microscopic objects, their mechanical quantum fluctuations are comparatively large, resulting in a very large optomechanical coupling strength. In combination with the ground-state cooling and quantum control techniques of atomic physics, this has allowed several experiments to enter the quantum regime of cavity optomechanics (Brennecke *et al.*, 2008; Murch *et al.*, 2008; Schleier-Smith *et al.*, 2011; Wolke *et al.*, 2012) and observe phenomena such as quantum measurement back-action (Murch *et al.*, 2008), ponderomotive squeezing (Brooks *et al.*, 2012), and novel many-body quantum phases (Baumann *et al.*, 2010). The field of cavity optomechanics with atoms has been reviewed in (Stamper-Kurn, 2014; Ritsch *et al.*, 2013).

9.5.1 'Atom-in-the-middle' Setup

As a simple model, we consider a cloud of N atoms in a trap of frequency Ω_a, which is placed in the standing-wave light field inside a Fabry–Perot optical cavity. This situation is closely analogous to cavity optomechanics experiments with thin dielectric membranes in optical cavities (Jayich *et al.*, 2008), see Fig. 9.3. Recall that the optomechanical single-photon single-phonon coupling constant in such a 'membrane-in-the-middle' setup is given by

$$g_0 = \frac{\partial \omega_{\text{cav}}}{\partial x} x_{\text{zpf}} = 2|r| \frac{\omega_{\text{cav}}}{L} x_{\text{zpf}} \tag{9.43}$$

where ω_{cav} is the resonance frequency and L the length of the cavity, and we have considered the case where the membrane of reflectivity r is placed on the slope of intracavity intensity standing wave, where g_0 is maximal.

To determine the optomechanical coupling for an 'atom-in-the-middle' system, we use the formalism of section 9.4 to calculate the reflectivity of the atoms. Note that in

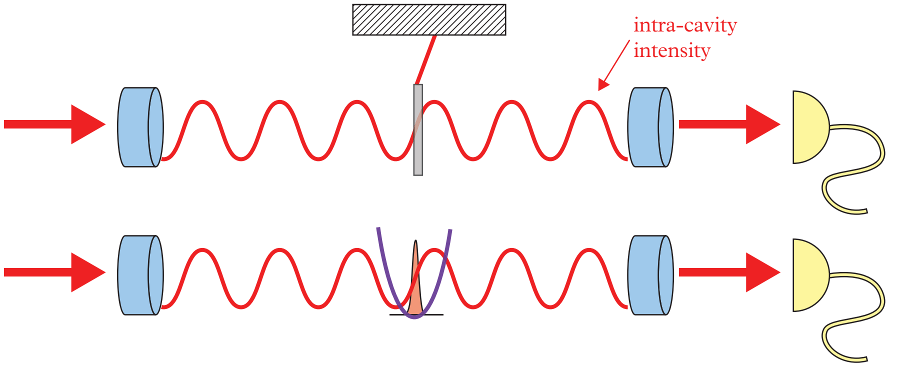

Fig. 9.3 *Analogy between a 'membrane-in-the-middle' setup (top) and an 'atom-in-the-middle' setup (bottom) for optomechanics. Figure courtesy of D. M. Stamper-Kurn.*

the regime where the atoms only weakly perturb the intracavity field ($|\zeta| \ll 1$), we have $r \simeq i\zeta$. For large detuning ($\Delta \gg \Gamma$), Eq. (9.36) gives a reflectivity of

$$|r| \simeq |\zeta| \simeq \frac{N\sigma}{2S} \cdot \frac{\Gamma}{2|\Delta|}. \tag{9.44}$$

The first term is half the resonant optical depth of the atoms, the second term accounts for the reduction of the atom–light interaction due to the detuning. Furthermore, since the mechanical mode of interest is the centre-of-mass motion of N atoms in the trap of frequency Ω_a, the zero-point motion has an amplitude of $x_{\text{zpf}} = \sqrt{\hbar/2Nm\Omega_a}$, where m is the mass of a single atom. Hence, the atom-optomechanical coupling constant can be expressed as

$$g_0 = \sqrt{N} \cdot \frac{\sigma}{S} \cdot \frac{\Gamma}{2|\Delta|} \cdot \frac{\omega_{\text{cav}}}{L} \sqrt{\frac{\hbar}{2m\Omega_a}}. \tag{9.45}$$

We find that the optomechanical coupling scales with $\sqrt{N}$, a characteristic feature of collective coupling. The same result can also be derived in the framework of cavity quantum electrodynamics in the dispersive limit, with N atoms collectively coupled to a single cavity mode (Stamper-Kurn, 2014). The interaction of the atomic centre-of-mass motion and the cavity mode is given by the generic optomechanical Hamiltonian (Aspelmeyer *et al.*, 2014)

$$H = \hbar\omega_{\text{cav}} c^\dagger c + \hbar\Omega_a a^\dagger a - \hbar g_0 c^\dagger c(a + a^\dagger), \tag{9.46}$$

again in direct analogy with a 'membrane-in-the-middle' setup. Here, c ($c^\dagger$) and a ($a^\dagger$) are annihilation (creation) operators for the photons of cavity mode and the phonons of the atomic centre-of-mass mode, respectively.

It is interesting to compare the parameters of an 'atom-in-the-middle' setup with those of a 'membrane-in-the-middle' experiment, see Table 9.2. Although the reflectivity of the atomic ensemble is very small, this is more than compensated for by the large atomic zero-point motion. As a result, the optomechanical coupling of the atomic system is several

Table 9.2 *Comparison of optomechanical coupling parameters for a Fabry–Perot cavity of length L containing, respectively, a micromechanical membrane and an ensemble of N atoms as mechanical element. For the atoms, we consider* $N = 5 \cdot 10^4$, $\Delta = 2\pi \cdot 100$ *GHz, and* $S = (30\ \mu\text{m})^2$.

	$\|r\|$	x_{zpf}	$\Omega/2\pi$	L	$g_0/2\pi$
membrane	0.4	$7 \cdot 10^{-16}$ m	270 kHz	1 mm	0.22 kHz
N atoms	$2 \cdot 10^{-4}$	$2 \cdot 10^{-10}$ m	50 kHz	200 μm	150 kHz

orders of magnitude bigger than that of a typical membrane-in-the-middle system. This feature, in combination with the established ground-state cooling and quantum control techniques of atomic physics, makes atomic systems attractive for exploring cavity optomechanics deep in the quantum regime.

9.5.2 Atom Optomechanics in the Quantum Regime

Several experimental implementations of cavity optomechanics with ultracold atoms have been reported (Brennecke *et al.*, 2008; Murch *et al.*, 2008; Purdy *et al.*, 2010; Schleier-Smith *et al.*, 2011; Brahms *et al.*, 2012; Wolke *et al.*, 2012), for a review see (Stamper-Kurn, 2014; Ritsch *et al.*, 2013).

In the experiments of the Berkeley group (Gupta *et al.*, 2007; Murch *et al.*, 2008; Purdy *et al.*, 2010; Brahms *et al.*, 2012), an ensemble of ultracold thermal ^{87}Rb atoms is tightly trapped in an optical lattice potential inside a high-finesse Fabry–Perot cavity. The lattice is realized by driving a cavity mode with a laser at a wavelength of 850 nm, far detuned from the atomic transition. The vibrations of the atoms in this far-detuned lattice interact with a second cavity mode at 780 nm, much closer to atomic resonance, see Fig. 9.4. Because the periodicities of the trapping mode and the probe mode are different, each lattice well experiences a different optomechanical coupling $g_0(z)$, where z is the position along the cavity axis. In contrast to the simplified picture presented above, the mechanical oscillator thus corresponds to a collective mode of the ensemble where each atomic cloud contributes with a weight given by the local optomechanical coupling. More recently, experiments have been performed with individual clouds (Purdy *et al.*, 2010), in direct analogy to the model of section 9.5.1. The mechanical mode is ground-state cooled using a combination of laser and evaporative cooling. This system has been used to observe optomechanical effects such as quantum measurement back-action (Murch *et al.*, 2008) and ponderomotive squeezing (Brooks *et al.*, 2012).

The large optomechanical coupling strength that can be achieved in atomic systems (see Table 9.2) opens the way to investigations of the 'granular' regime of optomechanics, where the interaction of phonons and photons is significant on the level of single quanta

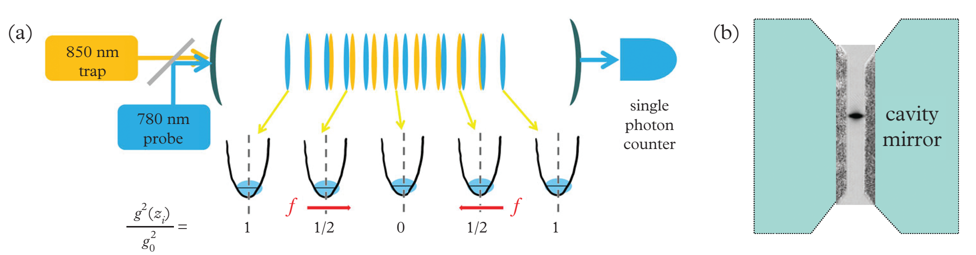

Fig. 9.4 *Optomechanics with atoms tightly confined in an intracavity lattice. (a) Schematic showing the intra-cavity optical lattice trap at 850 nm and the probe light at 780 nm. The mechanical mode is a collective oscillation of the array of atomic clouds. (b) Absorption image of the atoms between the mirrors of the optical cavity. Figure courtesy of D. M. Stamper-Kurn.*

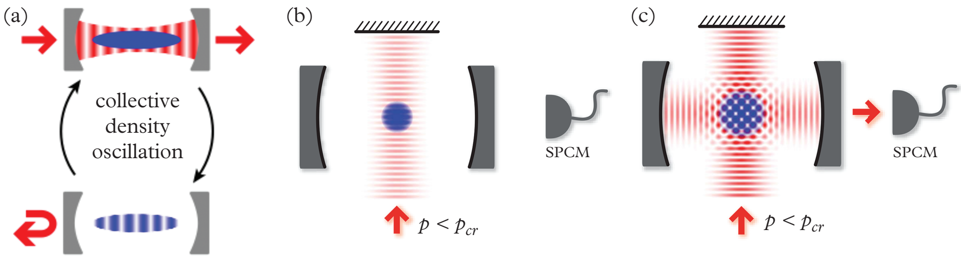

Fig. 9.5 *(a) Optomechanics with a weakly confined Bose–Einstein condensate. A collective density wave of the BEC acts as mechanical oscillator coupled to the cavity mode. (b,c) Setup used for the observation of the Dicke phase transition. (b) The gas is pumped from the side with light near-resonant with a cavity mode. (c) Above a certain threshold pump power, the atoms self-organize into a periodic pattern, maximizing the collective light scattering into the cavity mode. Figure courtesy of T. Esslinger.*

(Stamper-Kurn, 2014). The figure of merit is the ratio g_0/κ, where κ is the cavity linewidth. If $g_0/\kappa > 1$, a single phonon of vibration is sufficient to detune the cavity by more than its linewidth. Conversely, a single cavity photon gives a momentum kick to the mechanical oscillator that is larger than its zero-point momentum uncertainty. Experiments with atom-optomechanical systems are approaching the granular regime with $g_0/\kappa \sim 1$ (Brennecke *et al.*, 2008; Murch *et al.*, 2008), giving access to studies of nonlinear quantum optomechanics.

In the experiments of the Zürich group (Brennecke *et al.*, 2008), a Bose–Einstein condensate (BEC) is weakly trapped inside the cavity, distributed over many periods of the standing-wave cavity mode, see Fig. 9.5. In this system, the cavity mode is coupled to a collective density wave on the BEC, representing a mechanical oscillator of frequency $4\omega_r$, where $\omega_r = E_r/\hbar$ is the recoil frequency.

This experiment was used to explore optomechanical self-organization phenomena in many-body systems, such as the Dicke phase transition (Baumann *et al.*, 2010). When driven from the side with a standing-wave laser beam whose frequency is close to a cavity mode, the atoms can emit light into the cavity. Above a certain threshold driving strength, the atoms self-organize into a periodic pattern inside the cavity where they maximize their collective emission into the cavity mode and are simultaneously trapped by the combined cavity and driving laser field. These experiments open the path to studies of light–matter interactions at the intersection of optomechanics and many-body physics (Ritsch *et al.*, 2013).

9.6 Hybrid Mechanical-atomic Systems: Coupling Mechanisms

Hybrid mechanical systems are a promising way to achieve quantum control over the vibrations of mechanical oscillators (Treutlein *et al.*, 2014). In these systems, a mechanical oscillator is coupled to a microscopic quantum system for which a well-developed toolbox for quantum control is available. Through the coupling, this toolbox can be harnessed for enhanced cooling of mechanical structures, for detection of their quantum motion, for the preparation of non-classical states of vibration, and to implement new protocols for quantum measurement. In fact, the first experiment that reported a nanomechanical oscillator in the quantum regime used a hybrid approach (O'Connell *et al.*, 2010). More generally, since mechanical oscillators can be functionalized with electrodes, magnets and mirrors, they can couple to a variety of different quantum systems and serve as transducers in hybrid quantum information processing (Rabl *et al.*, 2010).

Different hybrid mechanical systems are currently being investigated, involving mechanical oscillators coupled to atoms (Wang *et al.*, 2006; Jöckel *et al.*, 2015; Camerer *et al.*, 2011; Hunger *et al.*, 2010; Montoya *et al.*, 2015), solid-state spin systems (Degen *et al.*, 2009; Arcizet *et al.*, 2011; Kolkowitz *et al.*, 2012; Teissier *et al.*, 2014; Ovartchaiyapong *et al.*, 2014), semiconductor quantum dots (Yeo *et al.*, 2013; Montinaro *et al.*, 2014), and superconducting qubits (O'Connell *et al.*, 2010; Pirkkalainen *et al.*, 2013; Lecocq *et al.*, 2015). Ultracold atoms are attractive in this context because all degrees of freedom, the internal states and the motion in a trap, can be controlled on the quantum level with long coherence times. In hybrid systems, the atoms can thus act as a microscopic mechanical oscillator deep in the quantum regime (Stamper-Kurn, 2014), or they can provide discrete internal levels that give access to new features difficult to realize in purely mechanical systems such as spin oscillators with negative effective mass (Hammerer *et al.*, 2009*a*; Polzik and Hammerer, 2015) and techniques for single-phonon control (Carmele *et al.*, 2014). Figure 9.6 shows an overview of different coupling

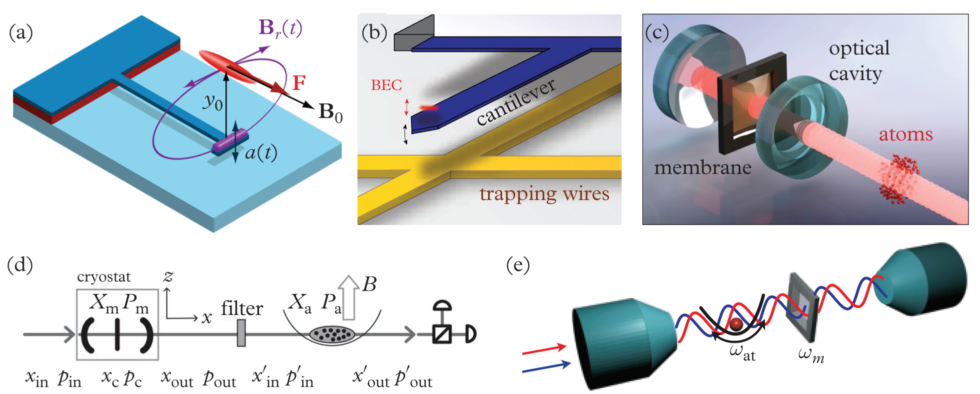

Fig. 9.6 *Coupling mechanisms for hybrid mechanical-atomic systems. (a) Cantilever with a magnetic tip coupled to the spin of atoms (Wang* et al.*, 2006; Treutlein* et al.*, 2007; Montoya* et al.*, 2015). (b) Cantilever coupled by atom-surface forces to the vibrations of a Bose–Einstein condensate in a trap (Hunger* et al.*, 2010). (c) Light-mediated coupling of a membrane oscillator to the vibrations of atoms in an optical lattice (Vogell* et al.*, 2013; Jöckel* et al.*, 2015). (d) Scheme for measurement-based entanglement generation between a membrane and the spin of an atomic ensemble (Hammerer* et al.*, 2009*a*). (e) Coupling of a membrane to the motion of a single atom through intracavity light fields (Hammerer* et al.*, 2009*b*).*

mechanisms for atoms and mechanical oscillators; see also the reviews in (Hunger *et al.*, 2011; Treutlein *et al.*, 2014)

First experimental implementations of hybrid mechanical-atomic systems in the classical regime were reported in (Wang *et al.*, 2006; Jöckel *et al.*, 2015; Camerer *et al.*, 2011; Hunger *et al.*, 2010; Montoya *et al.*, 2015). In (Wang *et al.*, 2006), a piezo-driven cantilever with a magnetic tip was used to excite magnetic resonance in a hot atomic vapour. In (Montoya *et al.*, 2015) a similar experiment was performed with trapped, ultracold atoms. In (Hunger *et al.*, 2010), a Bose–Einstein condensate was placed a few hundred nanometres from a classically driven cantilever, so that atom-surface forces led to the excitation of collective modes of the condensate. In all of these experiments, the atoms were used to detect classically driven mechanical vibrations at room temperature. However, the back-action of the atoms onto the mechanical oscillator, which is essential for controlling the oscillator with the atoms, could not be observed. More recently, hybrid mechanical-atomic systems coupled by light were implemented (Jöckel *et al.*, 2015; Camerer *et al.*, 2011). In these experiments, the back-action of the atoms onto the mechanical vibrations (Camerer *et al.*, 2011) as well as strong sympathetic cooling of the mechanical oscillator with the atoms (Jöckel *et al.*, 2015) were observed for the first time. Although the mechanical system still resided in the classical regime because of technical noise and its room-temperature environment, the experimental results showed good agreement with theory (Hammerer *et al.*, 2010*b*; Vogell *et al.*, 2013), which predicts that the quantum regime is accessible for realistic parameters.

In the following, we consider hybrid mechanical-atomic systems where the coupling is mediated by laser light. This results in a modular system, where the mechanical oscillator and the atoms reside in different experimental setups. The light can be routed from one setup to the other via a free-space link or an optical fibre. Such a modular setup circumvents the technological challenge of combining high-power lasers for atom trapping with a cryostat for pre-cooling of the mechanical device. Moreover, it is flexible, providing a great variety of coupling schemes, which can be implemented by simply changing the coupling laser configuration, without the need to open up the optomechanics setup or the cold atom machine. In particular, the light field can be arranged to couple either to the motion of the atoms (Hammerer *et al.*, 2010*b*; Vogell *et al.*, 2013) or to their internal state (Hammerer *et al.*, 2009*b*; Vogell *et al.*, 2015).

9.7 Optical Lattice with Vibrating Mirror

We consider a hybrid mechanical system as proposed in (Hammerer *et al.*, 2010*b*; Vogell *et al.*, 2013), in which the vibrations of a membrane oscillator are coupled via light to the centre-of-mass (c.o.m.) motion of ultracold atoms in an optical lattice. This system was experimentally realized in (Camerer *et al.*, 2011), where the coupling was studied and compared with theory. In a subsequent experiment, the coupling strength was strongly enhanced by placing the membrane in an optical cavity and sympathetic cooling of the membrane vibrations through their coupling to laser-cooled atoms was observed (Jöckel *et al.*, 2015).

9.7.1 Light-mediated Coupling

The coupled atom–membrane system is schematically shown in Fig. 9.7. Ultracold atoms are trapped in an optical lattice generated by reflecting a laser beam from an optomechanical system, essentially realizing an optical lattice with a vibrating mirror.

The optomechanical system is a Si_3N_4 membrane oscillator in an optical cavity in the 'membrane-in-the-middle' configuration (Thompson *et al.*, 2008; Jayich *et al.*, 2008). The Si_3N_4 film has a thickness of typically 50 nm and is supported by a Si frame, realizing a 'square drum' mechanical oscillator. For typical lateral dimensions of several hundred μm to a few mm such membranes feature vibrational modes with frequencies $\Omega_m/2\pi$ in the hundreds of kHz to few MHz range and very high mechanical quality factors of up to $Q = 5 \times 10^7$ (Wilson *et al.*, 2009; Jöckel *et al.*, 2011; Chakram *et al.*, 2014). In addition to their outstanding mechanical properties, these dielectric membranes also have very low optical absorption in the near infrared of order $10^{-5} - 10^{-6}$ in a single pass and a decent field reflectivity of typically $r_m = 0.4$.

The membrane is placed on the slope of the intracavity intensity standing wave. For concreteness, we consider the fundamental mode of the membrane, but coupling to higher-order modes can be realized in a similar way. As the membrane vibrates, it moves in and out of the intracavity field, periodically detuning the cavity resonance frequency ω_{cav}. This leads to an optomechanical coupling between the membrane vibrations and the intracavity field with single-photon single-phonon coupling constant

$$g_0 = G x_{\text{m,zpf}}, \tag{9.47}$$

where

$$G = -\frac{\partial \omega_{\text{cav}}}{\partial x} = 2|r_m| \frac{\omega_{\text{cav}}}{L} \tag{9.48}$$

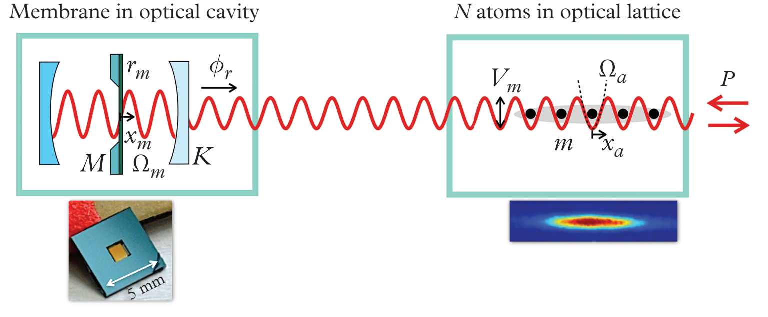

Fig. 9.7 *Atom-membrane coupling mediated by light. The vibrations x_m of a membrane in an optical cavity are coupled to the centre-of-mass motion x_a of an ensemble of N atoms in an optical lattice. The membrane cavity is single-sided and operates in the non-resolved sideband regime $\kappa \gg \Omega_m$. Atoms and membrane are placed in different experimental setups and coupled by light over a macroscopic distance.*

is the cavity frequency shift per membrane displacement, L is the cavity length, $x_{\mathrm{m,zpf}} = \sqrt{\hbar/2M\Omega_m}$ the zero-point amplitude and M the effective mass of the membrane mode.

The optical cavity is single-sided so that the light leaves the cavity again through the input port. Moreover, the cavity intensity decay rate $\kappa \gg \Omega_m$ so that the light leaving the cavity carries instantaneous information about the membrane displacement x_m. The cavity is resonantly driven by a laser of frequency $\omega_L = \omega_{\mathrm{cav}}$ and power P to a mean intracavity photon number

$$\bar{n}_c = \frac{4}{\kappa}\frac{P}{\hbar\omega_{\mathrm{cav}}}. \tag{9.49}$$

Under these conditions, the main effect of the membrane vibrations is to modulate the phase shift $\phi_r = \pi + \delta\phi_r$ of the beam reflected from the cavity by

$$\delta\phi_r = \frac{4}{\kappa}Gx_m. \tag{9.50}$$

The interference of the driving laser beam and the light reflected from the cavity creates an optical standing wave outside the cavity. If the driving laser is detuned from an atomic transition, this creates an optical lattice potential for the atoms as described in section 9.3. An ensemble of N atoms is trapped in this lattice and cooled to the ground state along the lattice direction with additional laser cooling beams. Each atom $i = 1 \ldots N$ experiences an optical lattice potential

$$U_i = V_m \cos^2\left(kx_{a,i} + \frac{\phi_r}{2}\right) \tag{9.51}$$

with modulation depth V_m given by Eq. (9.26). The lattice depends on the membrane position through ϕ_r. Expanding to second order in $kx_{a,i} \ll 1$ and $\delta\phi_r \ll 1$ around the potential minima we obtain

$$U_i \simeq V_m\left(kx_{a,i} + \frac{\delta\phi_r}{2}\right)^2 = V_m k^2 x_{a,i}^2 + V_m k x_{a,i}\delta\phi_r + V_m\left(\frac{\delta\phi_r}{2}\right)^2. \tag{9.52}$$

Using Eq. (9.50) and Eq. (9.28) for the trap frequency along the lattice we find

$$U_i \simeq \underbrace{\frac{1}{2}m\Omega_a^2 x_{a,i}^2}_{\text{atom trap}} + \underbrace{\frac{4}{\kappa}GV_m k x_{a,i} x_m}_{\text{coupling}} + \underbrace{V_m\left(\frac{2G}{\kappa}\right)^2 x_m^2}_{\text{freq. shift of membrane}}. \tag{9.53}$$

The first term is the atomic trapping potential in harmonic approximation, the second term describes a linear coupling of atomic and membrane motion, while the third term is a small correction to the membrane frequency that can be absorbed in the definition of Ω_m.

For N atoms trapped in the lattice, each atom experiences the optical potential and the resulting interaction Hamiltonian is $H_{\text{int}} = \sum_i H_i \sim x_m \sum_i x_{a,i}$ with H_i corresponding to the coupling term in Eq. (9.53). As a result, the membrane is coupled to the atomic c.o.m. coordinate $x_a = \frac{1}{N}\sum_i x_{a,i}$ with a Hamiltonian

$$H_{\text{int}} = N\frac{4}{\kappa}GV_m k x_a x_m. \tag{9.54}$$

Rewriting the position quadratures in terms of bosonic field operators

$$x_m = x_{\text{m,zpf}}(b+b^\dagger), \quad x_{\text{m,zpf}} = \sqrt{\frac{\hbar}{2M\Omega_m}}, \quad [b,b^\dagger] = 1 \tag{9.55}$$

for the membrane and

$$x_a = \frac{x_{\text{a,zpf}}}{\sqrt{N}}(a+a^\dagger), \quad x_{\text{a,zpf}} = \sqrt{\frac{\hbar}{2m\Omega_a}}, \quad [a,a^\dagger] = 1 \tag{9.56}$$

for the atomic c.o.m., we obtain the coupling Hamiltonian

$$H_{\text{int}} = \hbar g(b+b^\dagger)(a+a^\dagger) \tag{9.57}$$

with an atom-membrane single-phonon coupling constant

$$g = \sqrt{N}\,\frac{4g_0}{\kappa}\,\frac{V_m}{\hbar}\,kx_{\text{a,zpf}} \simeq |r_m|\Omega_a\sqrt{\frac{Nm}{M}}\,\frac{2\mathcal{F}}{\pi}, \tag{9.58}$$

where $\mathcal{F}$ is the cavity finesse and we have assumed near-resonant coupling $\Omega_a \approx \Omega_m$. Including the free evolution of membrane and atomic c.o.m., the full Hamiltonian is

$$H = \hbar\Omega_m b^\dagger b + \hbar\Omega_a a^\dagger a + \hbar g(b+b^\dagger)(a+a^\dagger). \tag{9.59}$$

We thus find that the light field acts like an optical ‘spring’ that couples the two mechanical oscillators, membrane and atoms. The coupling constant g in Eq. (9.58) contains a term $\sqrt{Nm/M}$, which is very small as the mass ratio of the atomic ensemble and the membrane is tiny (in the experiments of (Jöckel *et al.*, 2015), $Nm/M \approx 10^{-10}$). This can be understood as an impedance mismatch between the two mechanical oscillators. However, this small factor is compensated by the cavity finesse, which can be large ($\mathcal{F} = 10^3$–10^5). The cavity can be thought of as a ‘lever’ that impedance-matches the two mechanical oscillators.

The same interaction Hamiltonian can also be derived by considering the back-action of the atomic motion on the light field as in section 9.4. According to Eq. (9.42), the N atoms oscillating in the optical lattice potential modulate the power of the beam driving the optomechanical system by $\delta P = \frac{c}{2} F_{\text{dip}} = -cNV_m k^2 x_a$. This leads to a modulation of the intracavity photon number by $\delta \bar{n}_c = \frac{4}{\kappa} \frac{\delta P}{\hbar \omega_{\text{cav}}}$ and consequently to a modulation of the radiation pressure force acting on the membrane by $\delta F_{\text{rad}} = \hbar G \delta \bar{n}_c = -N \frac{4}{\kappa} G V_m k x_a$. This interaction gives rise to a Hamiltonian $H_{\text{int}} = N \frac{4}{\kappa} G V_m k x_a x_m$, in agreement with Eq. (9.54).

The simple semiclassical derivation of the atom-membrane coupling presented here is confirmed by a rigorous calculation using a fully quantum-mechanical description of atoms, membrane and light field (Vogell *et al.*, 2013). We point out that this coupling scheme can be implemented with a variety of different optomechanical systems featuring a single-sided cavity, such as the photonic crystal zipper cavities described in (Eichenfield *et al.*, 2009; Cohen *et al.*, 2013). A finite coupling efficiency to the membrane-cavity setup and losses in the optical beam path can be taken into account as in (Hammerer *et al.*, 2010*b*; Jöckel *et al.*, 2015).

9.7.2 Dissipation Mechanisms

In addition to the coherent coupling of atoms and membrane described by the Hamiltonian H in Eq. (9.59), there are a number of dissipation mechanisms that affect the atomic and membrane vibrations. As a result, the coupled system is described by a Lindblad master equation

$$\dot{\rho} = -\frac{i}{\hbar}[H, \rho] + \mathcal{L}_{\text{th}}\rho + \mathcal{L}_{\text{rp}}\rho + \mathcal{L}_{\text{a}}\rho + \mathcal{L}_{\text{a,cool}}\rho. \tag{9.60}$$

The dissipation mechanisms were derived in (Hammerer *et al.*, 2010*b*; Vogell *et al.*, 2013) and include the following contributions:

- **thermal heating of the membrane**

$$\mathcal{L}_{\text{th}}\rho = \frac{\Gamma_m}{2}(\bar{n}_{\text{th}} + 1) D[b]\rho + \frac{\Gamma_m}{2}\bar{n}_{\text{th}} D[b^\dagger]\rho. \tag{9.61}$$

  Here, $D[b]\rho = 2b\rho b^\dagger - b^\dagger b\rho - \rho b^\dagger b$ and similar for the other operators, $\bar{n}_{\text{th}} \simeq k_B T_{\text{env}}/\hbar\Omega_m$ is the membrane's thermal phonon occupation at environment temperature T_{env} and $\Gamma_m = \Omega_m/Q$ is the mechanical energy decay rate. Thermal heating results in a decoherence rate of the membrane vibrational ground state of $\Gamma_m \bar{n}_{\text{th}} = k_B T_{\text{env}}/\hbar Q$. Heating of the membrane due to absorption of the coupling light can be accounted for by an increase of T_{env}.

- **radiation-pressure noise on membrane**

$$\mathcal{L}_{\text{rp}}\rho = \frac{\Gamma_{\text{rp}}}{2} D[b]\rho + \frac{\Gamma_{\text{rp}}}{2} D[b^\dagger]\rho \tag{9.62}$$

Radiation-pressure shot noise leads to diffusion of the membrane motion with rate $\Gamma_{\rm rp} = 4g_0^2\bar{n}_c/\kappa$. This is a fundamental limitation for cooling of the membrane with the atoms. For small coupling laser power, $\Gamma_{\rm rp} \ll \Gamma_m \bar{n}_{\rm th}$ and thermal heating dominates.

- **recoil heating of atoms**

$$\mathcal{L}_{\rm a}\rho = \frac{\Gamma_{\rm heat}}{2} D[a]\rho + \frac{\Gamma_{\rm heat}}{2} D[a^\dagger]\rho \tag{9.63}$$

On the atomic side, spontaneous photon scattering and fluctuations of the dipole force lead to diffusion of the atomic motion in the lattice, as discussed in section 9.3.3, with a rate $\Gamma_{\rm heat}$ given in Eq. (9.30).

- **laser cooling of atoms**

$$\mathcal{L}_{\rm a,cool}\rho = \frac{\Gamma_{\rm a,cool}}{2}(\bar{n}_a + 1)D[a]\rho + \frac{\Gamma_{\rm a,cool}}{2}\bar{n}_a D[a^\dagger]\rho. \tag{9.64}$$

On the atomic system, additional laser cooling beams can be applied to continuously cool the atomic motion. This can be described by a cooling rate $\Gamma_{\rm a,cool}$ and a steady-state phonon occupation $\bar{n}_a$. Techniques such as Raman sideband cooling (Kerman *et al*., 2000; Treutlein *et al*., 2001) reach $\bar{n}_a < 1$. If furthermore $\Gamma_{\rm a,cool} \gg \Gamma_{\rm heat}$, the laser cooling is stronger than the additional heating due to the coupling lattice and the atoms remain in the ground state.

Depending on the strength of the coherent coupling g compared to the various dissipation rates, the coupled atom–membrane system shows different dynamics. In the following section 9.8, we first discuss how the atoms can be used for sympathetic cooling of the membrane vibrations. In section 9.9 we will discuss the regime of strong coherent coupling.

9.8 Sympathetic Cooling of a Membrane with Ultracold Atoms

In a recent experiment (Jöckel *et al*., 2015), the hybrid atom–membrane system discussed in the previous section was implemented and the atoms were used for sympathetic cooling of the membrane.

To act as an efficient coolant, the atoms must be laser cooled by external cooling beams, see Fig. 9.8, with a rate $\Gamma_{\rm a,cool} \gg (\Gamma_{\rm m}\bar{n}_{\rm th}, \Gamma_{\rm rp}, \Gamma_{\rm heat})$ that exceeds all other dissipation rates. For the parameters of the experiment, the atomic cooling rate was also larger than the coherent coupling, $\Gamma_{\rm a,cool} \gg g$. In this regime, the atom–membrane coherence is quickly damped and can be eliminated from the equations of motion. For $\Omega_a \approx \Omega_m$ we can furthermore make the rotating-wave approximation. Under these

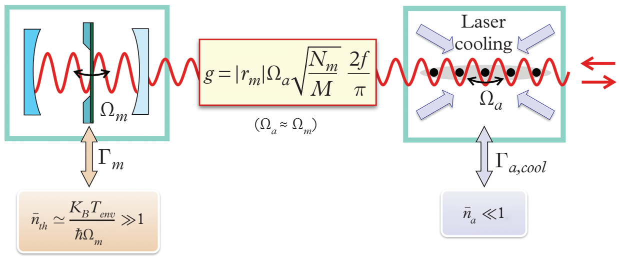

Fig. 9.8 *Sympathetic cooling of the membrane by coupling to laser-cooled atoms. Phonons enter the membrane with rate* $\Gamma_m \bar{n}_{th}$ *due to the coupling to the frame at temperature* T_{env}. *The light-mediated coupling* g *continuously transfers phonons between membrane and atoms. Phonons are removed from the coupled system by laser cooling the atoms with a set of laser cooling beams, corresponding to a coupling of the atoms with cooling rate* $\Gamma_{a,cool}$ *to a low-temperature bath* ($\bar{n}_a \ll 1$).

conditions, the master equation (9.60) yields the following coupled rate equations for the phonon occupations of the atomic c.o.m. and the membrane mode:

$$
\begin{aligned}
\frac{d}{dt}\langle a^\dagger a\rangle &= -\left(\Gamma_{a,cool} + \Gamma_{sym}\right)\langle a^\dagger a\rangle + \Gamma_{sym}\langle b^\dagger b\rangle + \Gamma_{heat} + \Gamma_{a,cool}\bar{n}_a, \\
\frac{d}{dt}\langle b^\dagger b\rangle &= -\left(\Gamma_m + \Gamma_{sym}\right)\langle b^\dagger b\rangle + \Gamma_{sym}\langle a^\dagger a\rangle + \Gamma_{rp} + \Gamma_m \bar{n}_{th}.
\end{aligned}
\tag{9.65}
$$

The rate at which the two systems exchange phonons is

$$
\Gamma_{sym} = \frac{4g^2}{\Gamma_{a,cool}}, \tag{9.66}
$$

which can be understood as the incoherent coupling of the membrane with rate g to the ultracold atomic reservoir of bandwidth $\Gamma_{a,cool} \gg g$. The membrane is sympathetically cooled at rate Γ_{sym}, while the atoms remain at low temperature due to the strong atomic laser cooling.

From Eqs. (9.65) we obtain the steady-state phonon occupation of the membrane

$$
\bar{n}_{ss} = \langle b^\dagger b\rangle_{ss} \simeq \frac{\Gamma_m \bar{n}_{th} + \Gamma_{rp}}{\Gamma_{sym} + \Gamma_m} + \frac{\Gamma_{sym}}{\Gamma_{sym} + \Gamma_m}\cdot\frac{\Gamma_{heat}}{\Gamma_{a,cool}} + \frac{\Gamma_{sym}}{\Gamma_{sym} + \Gamma_m}\cdot\bar{n}_a. \tag{9.67}
$$

The first term in this expression is the ratio of overall heating and cooling rates of the membrane, while the second and third term take into account the finite temperature of the atoms. Ground-state cooling of the membrane ($\bar{n}_{ss} \ll 1$) requires that

1. sympathetic cooling exceeds membrane heating, $\Gamma_{sym} \gg \Gamma_m \bar{n}_{th} + \Gamma_{rp}$,
2. the atoms are ground-state cooled, requiring $\Gamma_{a,cool} \gg \Gamma_{heat}$ and $\bar{n}_a \ll 1$.

We stress that unlike in standard cavity optomechanical cooling, the membrane-cavity system does *not* have to be in the resolved-sideband regime, i.e. sympathetic cooling with the atoms can reach the ground state for $\kappa \gg \Omega_m$. This can be understood by noting that the atomic oscillator provides the sideband resolution,[1] while the cavity simply enhances the optomechanical interaction. In section 9.9 we will see more generally that sympathetic cooling with atoms can reach the ground state in regimes where optomechanical techniques such as cavity cooling as well as feedback cooling (cold damping) fail to reach the ground state.

The sympathetic cooling scheme was implemented in a recent experiment (Jöckel *et al.*, 2015), where the membrane-cavity system was placed in a room-temperature environment. Figure 9.9 shows measurements of the membrane temperature as a function of time under different experimental conditions (Faber, 2016). If the coupling beam is turned on to sufficiently high power so that the atoms can resonantly couple to the membrane ($\Omega_a \approx \Omega_m$), the membrane temperature drops from $T_{\text{env}} = 300$ K to about $T_{\text{min}} = 600$ mK. The observed cooling rate extracted from the initial slope of the curve is $\Gamma_{\text{sym}} = 1.4 \times 10^3\ \text{s}^{-1}$. For comparison, if the coupling beam is turned on without any atoms in the lattice, the membrane temperature drops only to about 10 K. This is due to cavity optomechanical cooling, because the driving laser was slightly red-detuned from the cavity resonance to avoid the optomechanical instability on the blue-detuned side. If the coupling beam is turned off, the membrane stays at T_{env}.

The fact that the atoms cool the membrane by a factor of about $T_{\text{env}}/T_{\text{min}} = 500$ is rather remarkable if one recalls that the mass of the membrane is ten orders of magnitude larger than the mass of the entire atomic ensemble, $Nm/M \approx 10^{-10}$. Sympathetic cooling with laser-cooled atoms and atomic ions is frequently used to cool molecules or other atomic species that cannot be directly laser-cooled. In these experiments, the target and the coolant species thermalize through collisions, and a large mass ratio reduces the cooling efficiency. The largest particles that were cooled in this way are protein molecules in an ion trap, using laser-cooled Ba ions as the coolant (Offenberg *et al.*, 2008). These experiments involved mass ratios of up to ≈ 90 and achieved similar cooling factors and final temperatures as in the atom-membrane sympathetic cooling experiment.

In the proof-of-principle experiment of (Jöckel *et al.*, 2015), the membrane oscillator was placed in a room-temperature environment, resulting in a large thermal heating rate $\Gamma_{\text{m}}\bar{n}_{\text{th}} \gg \Gamma_{\text{sym}}$. The cooling performance was further limited by technical laser noise in the coupling beam, which was generated by a diode laser. To reach the quantum regime, the membrane can be pre-cooled in a cryostat, as in many other cavity-optomechanics experiments. Moreover, the use of higher-frequency membranes and low-noise lasers will mitigate the effects of technical laser noise. In the following section it is shown that with such an improved system, ground-state cooling and strong coupling of atoms and membrane are within reach.

[1] If the atoms are cooled by Raman sideband cooling we have $\bar{n}_a \approx (\Gamma_{\text{a,cool}}/4\Omega_a)^2$. The condition $\bar{n}_a \ll 1$ thus limits $\Gamma_{\text{a,cool}} \ll \Omega_a$, i.e. the atomic laser cooling must resolve the vibrational sidebands.

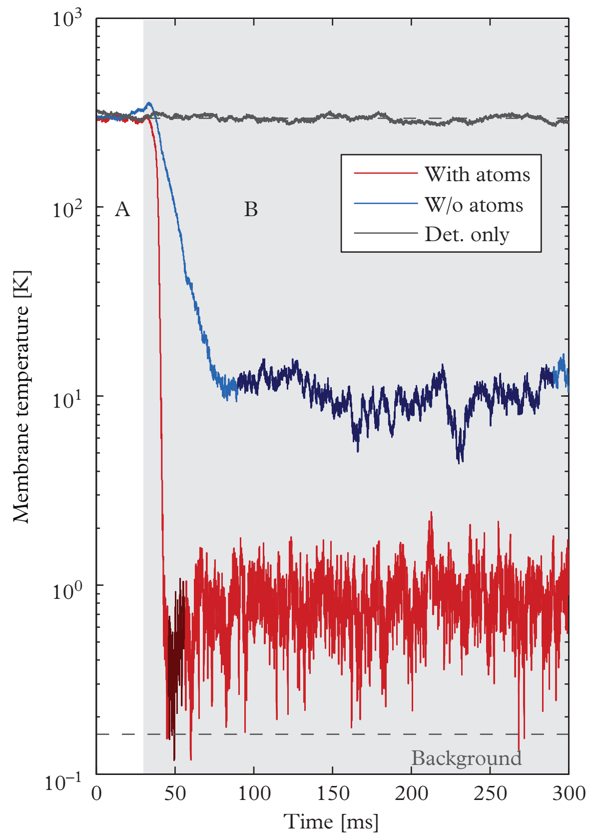

Fig. 9.9 *Sympathetic cooling results. The membrane temperature is shown as a function of time. In the grey-shaded region, the lattice laser beam is turned on so that the atoms can resonantly couple to the membrane,* $\Omega_a \approx \Omega_m$. *Red data: measurement with atoms in the lattice, showing strong sympathetic cooling. Blue: measurement without atoms, showing cavity optomechanical cooling. Black: lattice laser turned off. Figure courtesy of A. Faber.*

9.9 Ground-state Cooling, Strong Coupling, Cooperativity

In this section we discuss the conditions for observing quantum effects in the coupled atom–membrane system. We find that the atom–membrane cooperativity is an important figure of merit of the coupled system. We conclude by providing a set of parameters for which the system reaches the regime of large cooperativity.

9.9.1 Atom-Membrane Cooperativity

Figure 9.10 shows a schematic of the coupled atom–membrane system and its interaction with the environment. The strength of the coherent coupling is quantified by the rate

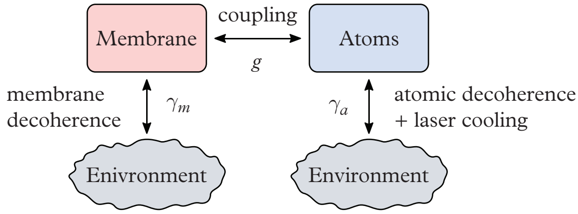

Fig. 9.10 *Coherent coupling and decoherence rates in the coupled atom–membrane system.*

g given in Eq. (9.58). On the membrane side, we define the decoherence rate of the vibrational ground state

$$\gamma_m = \Gamma_{\mathrm{m}} \bar{n}_{\mathrm{th}} + \Gamma_{\mathrm{rp}}. \tag{9.68}$$

For the atoms, the ground-state decoherence rate depends on whether laser cooling is applied (since typically $\Gamma_{\mathrm{a,cool}} \gg \Gamma_{\mathrm{heat}}$),

$$\gamma_a = \Gamma_{\mathrm{heat}} + \Gamma_{\mathrm{a,cool}} \simeq \begin{cases} \Gamma_{\mathrm{a,cool}} & \text{if laser cooling is on} \\ \Gamma_{\mathrm{heat}} & \text{otherwise.} \end{cases} \tag{9.69}$$

We now define the atom–membrane cooperativity

$$\mathcal{C} = \frac{4g^2}{\gamma_m \gamma_a}, \tag{9.70}$$

which compares the strength of the coherent interaction with the product of the decoherence rates of the two systems. In analogy with the corresponding parameter in cavity quantum electrodynamics (Tanji-Suzuki *et al.*, 2011) or cavity optomechanics (Aspelmeyer *et al.*, 2014), we expect the cooperativity to be the relevant figure of merit when analysing the ability of the system to show certain quantum effects.

Ground-state cooling

As a first example, we consider again ground-state cooling of the membrane by coupling to laser-cooled atoms as described in the previous section. Assuming that the atoms are ground-state cooled and focusing on the experimentally relevant regime of $\Gamma_{\mathrm{sym}} \gg \Gamma_{\mathrm{m}}$, we can express the steady-state phonon occupation of the membrane Eq. (9.67) as

$$\bar{n}_{\mathrm{ss}} \simeq \frac{\gamma_m}{\Gamma_{\mathrm{sym}}} = \frac{\gamma_m \Gamma_{\mathrm{a,cool}}}{4g^2} = \frac{1}{\mathcal{C}}. \tag{9.71}$$

Ground-state cooling of the membrane ($\bar{n}_{\mathrm{ss}} < 1$) thus requires a cooperativity $\mathcal{C} > 1$.

Strong coupling

For balanced decoherence rates $\gamma_a \approx \gamma_m$, the condition $C > 1$ implies $g > (\gamma_a/2, \gamma_m/2)$. This is the strong-coupling regime as defined e.g. in cavity quantum electrodynamics (Tanji-Suzuki *et al.*, 2011), where single-phonon Rabi oscillations can be observed and a quantum state swap between the two systems is possible.

Effects analogous to electromagnetically induced transparency

If $\mathcal{C} > 1$ but we either have $g < \gamma_a/2$ or $g < \gamma_m/2$, a full single-phonon Rabi oscillation between the two systems cannot be observed in the time domain, but interference phenomena analogous to electromagnetically induced transparency are still observable and can be exploited for coherent control.

9.9.2 Connection to Optomechanical Cooperativity and Optical Depth

We can express the atom–membrane coupling Eq. (9.58) as

$$g = \frac{4\sqrt{N}\bar{n}_c g_0 g_a}{\kappa}, \tag{9.72}$$

where g_0 is the membrane–light and $g_a = V_1 k x_{\mathrm{a,zpf}}/\hbar$ the atom–light coupling strength for a single photon in the cavity. Here, $V_1 = V_m/\bar{n}_c$ is the lattice potential experienced by the atoms for a single photon in the cavity.[2] We furthermore assume $\gamma_m \simeq \Gamma_{\mathrm{m}}\bar{n}_{\mathrm{th}}$ and $\gamma_a \simeq \Gamma_{\mathrm{heat}}$. With this we can express the atom–membrane cooperativity as

$$\mathcal{C} = \frac{4g^2}{\gamma_m\gamma_a} = 4 \cdot \frac{4g_0^2\bar{n}_c}{\kappa\Gamma_{\mathrm{m}}\bar{n}_{\mathrm{th}}} \cdot \frac{4g_a^2\bar{n}_c N}{\kappa\Gamma_{\mathrm{heat}}} = 4\mathcal{C}_m\mathcal{C}_a, \tag{9.73}$$

where the optomechanical (quantum) cooperativity referring to the membrane–light interaction is defined in the usual way (Aspelmeyer *et al.*, 2014),

$$\mathcal{C}_m = \frac{4g_0^2\bar{n}_c}{\kappa\Gamma_{\mathrm{m}}\bar{n}_{\mathrm{th}}}. \tag{9.74}$$

The atomic cooperativity referring to the atom–light interaction is

$$\mathcal{C}_a = \frac{4g_a^2\bar{n}_c N}{\kappa\Gamma_{\mathrm{heat}}} = N\frac{\sigma}{S}, \tag{9.75}$$

[2] Note that the atoms are trapped in a lattice outside the cavity, but the power of the lattice beam and the intracavity photon number are related by Eq. (9.49).

which is simply the resonant optical depth of the atomic ensemble, as expected for a free-space atom–light interface (Tanji-Suzuki *et al.*, 2011; Hammerer *et al.*, 2010*a*). To derive the second equality in Eq. (9.75) we have used Eqs. (9.26), (9.29), (9.30), and (9.49).

Equation (9.73) implies that the coupled atom–membrane system can operate in a regime of large cooperativity $\mathcal{C} > 1$ even if the optomechanical system has a cooperativity $\mathcal{C}_m < 1$, because this can be compensated for by a large resonant optical depth $\mathcal{C}_a$, which can reach hundreds or thousandths in state-of-the-art experiments. This has interesting consequences, as it implies that ground-state cooling and quantum control of the membrane by coupling to atoms is possible in the regime $\mathcal{C}_m < 1$, where standard optomechanical techniques applied to the membrane–cavity system alone, i.e. without atoms in the beam path, cannot achieve these tasks.

For example, as discussed in (Bennett *et al.*, 2014), optomechanical ground-state cooling (without atoms) requires $\mathcal{C}_m > \frac{1}{8}$ (feedback cooling/cold damping) or $\mathcal{C}_m > 1$ (cavity feedback cooling). If neither of these conditions is fulfilled, the membrane can still be ground-state cooled by coupling it to an ensemble of laser-cooled atoms with $\mathcal{C}_a \gg 1$ such that the overall cooperativity $\mathcal{C} = 4\mathcal{C}_m\mathcal{C}_a > 1$. This can be understood in terms of the concept of quantum feedback (Bennett *et al.*, 2014): the atoms can be considered a coherent controller that can potentially outperform a classical controller that uses detection of light from the cavity and classical feedback. The hybrid atom–membrane setup thus allows one to experimentally study intriguing conceptual questions on the remote control of a quantum system (the mechanical oscillator) with the help of another quantum system (the atoms).

9.9.3 Experimental Parameters

In this section we give a set of experimental parameters of the coupled atom–membrane system for which the regime of large cooperativity and strong coupling is reached.

We consider the (3, 3)-mode of a standard Si_3N_4 membrane of dimensions 1.5 mm × 1.5 mm × 50 nm with $r_m = 0.4$ and mechanical frequency $\Omega_m/2\pi = 0.8$ MHz, effective mass $M = 80$ ng, and quality factor $Q = 1 \times 10^7$, mounted in a cryostat at $T_{\text{env}} = 4$ K. The membrane is placed in an optical cavity of length $L = 1$ mm and finesse $\mathcal{F} = 2 \times 10^3$. The cavity is driven with a laser of power $P = 190$ μW, cross-sectional area $S = (25\ \mu\text{m})^2$, and detuning $\Delta/2\pi = 5$ GHz from the D_2 line of ^{87}Rb atoms. This generates an optical lattice potential with $\Omega_a = \Omega_m$ where we assume $N = 1 \times 10^6$ atoms are trapped.

For this system we find a coupling strength of $g = 1.2 \times 10^5\ \text{s}^{-1}$, to be compared with decoherence rates $\Gamma_\text{m}\bar{n}_\text{th} = 8 \times 10^4\ \text{s}^{-1}$ and $\Gamma_a = 1.6 \times 10^3\ \text{s}^{-1}$, placing the system in the strong-coupling regime. For the cooperativities we find $\mathcal{C}_m = 0.5$, $\mathcal{C}_a = 310$, and $\mathcal{C} = 643$.

9.10 Coupling to the Atomic Internal State

By coupling the mechanical vibrations to the atomic internal state, the full toolbox of quantum control in atomic ensembles becomes accessible (Hammerer *et al.*, 2010*a*).

Such a coupling can be achieved in a setup very similar to Fig. 9.7, as shown in (Vogell *et al.*, 2015). The basic idea is to transduce the mechanical vibrations into a polarization rotation of the coupling light that couples to the atomic hyperfine spin. Conversely, changes in the atomic hyperfine state change the light polarization and modulate the radiation pressure on the mechanics. This again gives rise to a Hamiltonian of the form (Vogell *et al.*, 2015)

$$H = \hbar\Omega_m b^\dagger b + \hbar\omega_L a^\dagger a + \hbar g_{\text{int}}(b + b^\dagger)(a + a^\dagger), \tag{9.76}$$

similar to Eq. (9.59), except that a and $a^\dagger$ now refer to excitations of the atomic spin state and ω_L is the Larmor frequency. We have assumed that the collective spin describing the internal state of the N atoms is polarized along a magnetic field so that it can be mapped to a harmonic oscillator, $S_z \simeq a^\dagger a - N/2$ and $S_x \simeq \sqrt{N/2}\left(a + a^\dagger\right)$ in the Holstein–Primakoff approximation (Hammerer *et al.*, 2010*a*). Several schemes have been analysed that give rise to such interactions (Hammerer *et al.*, 2009*a*; Bariani *et al.*, 2014; Vogell *et al.*, 2015) and strong coupling has been predicted for realistic parameters (Vogell *et al.*, 2015). Since the Larmor frequency ω_L can be tuned with magnetic fields over a wide range, the atoms can be coupled to mechanical oscillators in the MHz regime, where laser and other technical noise is much reduced.

9.10.1 Beam Splitter and Two-mode Squeezing Hamiltonians

Different types of interactions can be realized with this Hamiltonian: by magnetic-field tuning of the Larmor frequency to $\omega_L = \Omega_m$, the resonant interactions take the form of a 'beam-splitter' Hamiltonian $H_{\text{int}} = \hbar g_{\text{int}}\left(ba^\dagger + b^\dagger a\right)$, giving rise to normal mode splitting and Rabi oscillations between the mechanical and atomic system. This can be used to swap spin-squeezed and other non-classical states of the atoms to the mechanical system (Riedel *et al.*, 2010). Alternatively, by inverting the magnetic field orientation one can set $\omega_L = -\Omega_m$, so that $H_{\text{int}} = \hbar g_{\text{int}}\left(ba + b^\dagger a^\dagger\right)$. This 'two-mode squeezing' Hamiltonian produces entanglement between the atomic and mechanical modes. Interestingly, in this case the atomic ensemble can be thought of as realizing a spin oscillator with a 'negative effective mass' (Polzik and Hammerer, 2015), since $\omega_L < 0$ and creating atomic excitations thus reduces the energy. This illustrates one of the new features that atoms can provide in such hybrid systems.

9.10.2 Vibration Sensing beyond the Standard Quantum Limit

The two-mode squeezing Hamiltonian can be used to generate Einstein–Podolsky–Rosen entanglement between the mechanical oscillator and the atoms. As pointed out in (Hammerer *et al.*, 2009*a*), this can be used for sensing of mechanical vibrations beyond the standard quantum limit, which limits the precision of weak continuous position measurements (Aspelmeyer *et al.*, 2014). Entanglement is present if the variances of position and moment measurements on the two systems satisfy (Polzik and Hammerer, 2015)

$$\mathrm{Var}(X_m - X_a) + \mathrm{Var}(P_m + P_a) < 2, \tag{9.77}$$

where X_m (X_a) and P_m (P_a) here refer to dimensionless position and momentum quadratures of the mechanical oscillator (atoms), defined such that they satisfy the commutation relation $[X_m, P_m] = i$ ($[X_a, P_a] = i$). In the entangled state, a position (momentum) measurement on the atomic system can predict the outcome of a position (momentum) measurement on the mechanical system with a precision better than the SQL. Remarkably, this holds for both position and momentum quadratures. This distinguishes the approach from other schemes of back-action evasion in mechanical systems, which are limited to a single quadrature. It was pointed out (Polzik and Hammerer, 2015) that this allows one to follow trajectories of the mechanical system in the reference frame provided by the atoms in principle without quantum uncertainty. A further exciting aspect is that this is possible in a remote way, with atoms placed at a macroscopic distance from the mechanical oscillator.

9.10.3 Single-phonon Control

Exploiting the coupling of the mechanical oscillator to the atomic internal state can also be used to obtain control over single phonons. In the atomic ensemble, the effect of Rydberg blockade can be used to restrict the internal-state dynamics to an effective two-level system (Saffman *et al.*, 2010; Weber *et al.*, 2015). Creating single excitations of the atomic ensemble in this way and swapping them to the mechanical system provides a challenging, but in principle feasible, route to controlling single phonon excitations in hybrid mechanical–atomic systems. Indeed, a recent proposal suggests making use of Rydberg excitations in small atomic ensembles to achieve the desired nonlinearities and identifies a parameter regime for such experiments (Carmele *et al.*, 2014).

Bibliography

Adams, C. S. and Riis, E. (1997). Laser cooling and trapping of neutral atoms. *Prog. Quant. Electr.*, **21**(1), 1–79.

Arcizet, O., Jacques, V., Siria, A., Poncharal, P., Vincent, P., and Seidelin, S. (2011, September). A single nitrogen-vacancy defect coupled to a nanomechanical oscillator. *Nature Physics*, 7(11), 879–83.

Asboth, J. K., Ritsch, H., and Domokos, P. (2008). Optomechanical coupling in a one-dimensional optical lattice. *Physical Review A*, 77, 063424.

Aspelmeyer, M., Kippenberg, T. J., and Marquardt, F. (2014, December). Cavity optomechanics. *Rev. Mod. Phys.*, **86**, 1391.

Aspelmeyer, M., Meystre, P., and Schwab, K. (2012). Quantum optomechanics. *Physics Today*, **65**(7), 29.

Bariani, F., Singh, S., Buchmann, L. F., Vengalattore, M., and Meystre, P. (2014, September). Hybrid optomechanical cooling by atomic lambda systems. *Physical Review A*, **90**(3), 033838.

Baumann, K., Guerlin, C., Brennecke, F., and Esslinger, T. (2010, April). Dicke quantum phase transition with a superfluid gas in an optical cavity. *Nature*, **464**(7293), 1301–6.

Bennett, J. S., Madsen, L. S., Baker, M., Rubinsztein-Dunlop, H., and Bowen, W. P. (2014). Coherent control and feedback cooling in a remotely-coupled hybrid atom-optomechanical system. *New Journal of Physics*, **16**(8), 083036.

Bloch, I. (2005). Ultracold quantum gases in optical lattices. *Nature Physics*, **1**(1), 23.

Brahms, N., Botter, T., Schreppler, S., Brooks, D. W. C., and Stamper-Kurn, D. M. (2012, March). Optical detection of the quantization of collective atomic motion. *Physical Review Letters*, **108**(1), 133601.

Brennecke, F., Ritter, S., Donner, T., and Esslinger, T. (2008). Cavity optomechanics with a Bose–Einstein condensate. *Science*, **322**(5899), 235.

Brooks, D. W. C., Botter, T., Schreppler, S., Purdy, T. P., Brahms, N., and Stamper-Kurn, D. M. (2012, August). Non-classical light generated by quantum-noise-driven cavity optomechanics. *Nature*, **488**(7412), 476–80.

Camerer, S., Korppi, M., Jöckel, A., Hunger, D., Hänsch, T. W., and Treutlein, P. (2011, November). Realization of an optomechanical interface between ultracold atoms and a membrane. *Physical Review Letters*, **107**(22), 223001.

Carmele, A., Vogell, B., Stannigel, K., and Zoller, P. (2014, June). Opto-nanomechanics strongly coupled to a Rydberg superatom: coherent versus incoherent dynamics. *New Journal of Physics*, **16**(6), 063042.

Chakram, S., Patil, Y. S., Chang, L., and Vengalattore, M. (2014, March). Dissipation in ultrahigh quality factor SiN membrane resonators. *Physical Review Letters*, **112**(12), 127201.

Chu, S. (1991). Laser manipulation of atoms and particles. *Science*, **253**, 861.

Chu, S. (2002, March). Cold atoms and quantum control. *Nature*, **416**(6), 206–10.

Cohen, J. D., Meenehan, S. M., and Painter, O. (2013). Optical coupling to nanoscale optomechanical cavities for near quantum-limited motion transduction. *Optics Express*, **21**(9), 11227–36.

Degen, C. L., Poggio, M., Mamin, H. J., Rettner, C. T., and Rugar, D. (2009, February). Nanoscale magnetic resonance imaging. *Proceedings of the National Academy of Sciences*, **106**(5), 1313–17.

Eichenfield, M., Camacho, R., Chan, J., Vahala, K. J., and Painter, O. (2009, May). A picogram- and nanometre-scale photonic-crystal optomechanical cavity. *Nature*, **459**(7246), 550–5.

Faber, A. (2016). *Sympathetic cooling and self-oscillations in a hybrid atom-membrane system*. Ph.D. thesis, University of Basel.

Feynman, R. P., Leighton, R. B., and Sands, M. (1964). *The Feynman Lectures on Physics*. Volume 1. Addison-Wesley.

Genes, C., Ritsch, H., Drewsen, M., and Dantan, A. (2011, November). Atom-membrane cooling and entanglement using cavity electromagnetically induced transparency. *Physical Review A*, **84**(5), 051801.

Gordon, J. P. and Ashkin, A. (1980). Motion of atoms in a radiation trap. *Physical Review A*, **21**(5), 1606–17.

Görlitz, A., Weidemüller, M., Hänsch, T. W., and Hemmerich, A. (1997). Observing the position spread of atomic wave packets. *Physical Review Letters*, **78**(11), 2096–9.

Grimm, R., Weidemüller, M., and Ovchinnikov, Y. B. (2000). Optical dipole traps for neutral atoms. *Adv. At. Mol. Opt. Phys*, **42**, 95.

Gross, C., Zibold, T., Nicklas, E., Estève, J., and Oberthaler, M. K. (2010, March). Nonlinear atom interferometer surpasses classical precision limit. *Nature*, **464**(7292), 1165.

Gupta, S., Moore, K. L., Murch, K. W., and Stamper-Kurn, D. M. (2007, November). Cavity nonlinear optics at low photon numbers from collective atomic motion. *Physical Review Letters*, **99**(21), 213601.

Hammerer, K., Aspelmeyer, M., Polzik, E., and Zoller, P. (2009*a*, January). Establishing Einstein–Poldosky–Rosen channels between nanomechanics and atomic ensembles. *Physical Review Letters*, **102**(2), 020501.

Hammerer, K., Sørensen, A. S., and Polzik, E. S. (2010*a*). Quantum interface between light and atomic ensembles. *Reviews of Modern Physics*, **82**(2), 1041–93.

Hammerer, K., Stannigel, K., Genes, C., Zoller, P., Treutlein, P., Camerer, S., Hunger, D., and Hänsch, T. W. (2010*b*, August). Optical lattices with micromechanical mirrors. *Physical Review A*, **82**(2), 021803.

Hammerer, K., Wallquist, M., Genes, C., Ludwig, M., Marquardt, F., Treutlein, P., Zoller, P., Ye, J., and Kimble, H. J. (2009*b*, August). Strong coupling of a mechanical oscillator and a single atom. *Physical Review Letters*, **103**(6), 63005.

Hunger, D., Camerer, S., Hänsch, T. W., König, D., Kotthaus, J. P., Reichel, J., and Treutlein, P. (2010, April). Resonant coupling of a Bose–Einstein condensate to a micromechanical oscillator. *Physical Review Letters*, **104**(1), 143002.

Hunger, D., Camerer, S., Korppi, M., Jöckel, A., Hänsch, T. W., and Treutlein, P. (2011, August). Coupling ultracold atoms to mechanical oscillators. *Comptes Rendus Physique*, **12**, 871.

Jayich, A. M., Sankey, J. C., Zwickl, B. M., Yang, C., Thompson, J. D., Girvin, S. M., Clerk, A. A., Marquardt, F., and Harris, J. G. E. (2008, September). Dispersive optomechanics: a membrane inside a cavity. *New Journal of Physics*, **10**(9), 095008.

Jöckel, A., Faber, A., Kampschulte, T., Korppi, M., Rakher, M. T., and Treutlein, P. (2015, January). Sympathetic cooling of a membrane oscillator in a hybrid mechanical–atomic system. *Nature Nanotechnology*, **10**(1), 55–9.

Jöckel, A., Rakher, M. T., Korppi, M., Camerer, S., Hunger, D., Mader, M., and Treutlein, P. (2011). Spectroscopy of mechanical dissipation in micro-mechanical membranes. *Appl. Phys. Lett.*, **99**(14), 143109.

Kerman, A. J., Vuletic, V., Chin, C., and Chu, S. (2000). Beyond optical molasses: 3D Raman sideband cooling of atomic cesium to high phase-space density. *Physical Review Letters*, **84**(3), 439–42.

Kolkowitz, S., Bleszynski Jayich, A. C., Unterreithmeier, Q. P., Bennett, S. D., Rabl, P., Harris, J. G. E., and Lukin, M. D. (2012, March). Coherent sensing of a mechanical resonator with a single-spin qubit. *Science*, **335**(6076), 1603–6.

Kozuma, M., Nakagawa, K., Jhe, W., and Ohtsu, M. (1996). Observation of temporal behavior of an atomic wave packet localized in an optical potential. *Physical Review Letters*, **76**(14), 2428–31.

Lecocq, F., Teufel, J. D., Aumentado, J., and Simmonds, R. W. (2015, June). Resolving the vacuum fluctuations of an optomechanical system using an artificial atom. *Nature Physics*, **11**(8), 635–639.

McConnell, R., Zhang, H., Hu, J., Ćuk, S., and Vuletic, V. (2015, March). Entanglement with negative Wigner function of almost 3,000 atoms heralded by one photon. *Nature*, **519**(7544), 439–42.

Miller, R., Northup, T. E., Birnbaum, K. M., Boca, A., Boozer, A. D., and Kimble, H. J. (2005, February). Trapped atoms in cavity QED: coupling quantized light and matter. *Journal of Physics B Atomic Molecular and Optical Physics*, **38**, S551.

Montinaro, M., Wust, G., Munsch, M., Fontana, Y., Russo-Averchi, E., Heiss, M., Fontcuberta i Morral, A., Warburton, R. J., and Poggio, M. (2014, August). Quantum dot opto-mechanics in a fully self-assembled nanowire. *Nano Letters*, **14**(8), 4454–60.

Montoya, C., Valencia, J., Geraci, A. A., Eardley, M., Moreland, J., Hollberg, L., and Kitching, J. (2015). Resonant interaction of trapped cold atoms with a magnetic cantilever tip. *Physical Review A*, **91**(6), 063835.

Murch, K., Moore, K., Gupta, S., and Stamper-Kurn, D. M. (2008). Observation of quantum-measurement backaction with an ultracold atomic gas. *Nature Physics*, **4**, 561.

O'Connell, A. D., Hofheinz, M., Ansmann, M., Bialczak, R. C., Lenander, M., Lucero, E., Neeley, M., Sank, D., Wang, H., Weides, M., Wenner, J., Martinis, J. M., and Cleland, A. N. (2010, March). Quantum ground state and single-phonon control of a mechanical resonator. *Nature*, **464**, 697.

Offenberg, D., Zhang, C., Wellers, Ch., Roth, B., and Schiller, S. (2008, December). Translational cooling and storage of protonated proteins in an ion trap at subkelvin temperatures. *Physical Review A*, 78(6), 061401.

Ovartchaiyapong, P., Lee, K. W., Myers, B. A., and Bleszynski Jayich, A. C. (2014, July). Dynamic strain-mediated coupling of a single diamond spin to a mechanical resonator. *Nature Communications*, **5**, 4429.

Pirkkalainen, J. M., Cho, S. U., Li, J., Paraoanu, G. S., Hakonen, P. J., and Sillanpää, M. A. (2013, February). Hybrid circuit cavity quantum electrodynamics with a micromechanical resonator. *Nature*, **494**(7436), 211–15.

Polzik, E. S. and Hammerer, K. (2015, January). Trajectories without quantum uncertainties. *Annalen der Physik*, **527**(1–2), A15–A20.

Purdy, T. P., Brooks, D. W. C., Botter, T., Brahms, N., Ma, Z. Y., and Stamper-Kurn, D. M. (2010). Tunable cavity optomechanics with ultracold atoms. *Physical Review Letters*, **105**(13), 133602.

Rabl, P., Harris, J. G. E., Zoller, P., and Lukin, M. D. (2010, May). A quantum spin transducer based on nanoelectromechanical resonator arrays. *Nature Physics*, **6**(8), 602.

Raithel, G., Phillips, W. D., and Rolston, S. L. (1998). Collapse and revivals of wave packets in optical lattices. *Physical Review Letters*, **81**(17), 3615.

Riedel, M. F., Böhi, P. A., Li, Y., Hänsch, T. W., Sinatra, A., and Treutlein, P. (2010, March). Atom-chip-based generation of entanglement for quantum metrology. *Nature*, **464**(7292), 1170.

Ritsch, H., Domokos, P., Brennecke, F., and Esslinger, T. (2013, April). Cold atoms in cavity-generated dynamical optical potentials. *Reviews of Modern Physics*, **85**(2), 553–601.

Romero-Isart, O., Pflanzer, A. C., Juan, M. L., Quidant, R., Kiesel, N., Aspelmeyer, M., and Cirac, J. I. (2011, January). Optically levitating dielectrics in the quantum regime: Theory and protocols. *Physical Review A*, **83**(1), 013803.

Saffman, M., Walker, T.G., and Mølmer, K. (2010). Quantum information with Rydberg atoms. *Reviews of Modern Physics*, **82**(3), 2313.

Schleier-Smith, M. H., Leroux, I. D., Zhang, H., Van Camp, M. A., and Vuletic, V. (2011, September). Optomechanical cavity cooling of an atomic ensemble. *Physical Review Letters*, **107**(14), 143005.

Stamper-Kurn, D. M. (2014). Cavity optomechanics with cold atoms. In *Cavity Optomechanics* (ed. M. Aspelmeyer, T. Kippenberg, and F. Marquardt), pp. 283–325. Springer, Berlin, Heidelberg.

Tanji-Suzuki, H., Leroux, I. D., Schleier-Smith, M. H, Cetina, M., Grier, A. T., Simon, J., and Vuletic, V. (2011). Interaction between atomic ensembles and optical resonators: Classical Description. *Advances in Atomic, Molecular and Optical Physics*, **60**, 201–37.

Teissier, J., Barfuss, A., Appel, P., Neu, E., and Maletinsky, P. (2014, July). Strain coupling of a nitrogen-vacancy center spin to a diamond mechanical oscillator. *Physical Review Letters*, **113**(2), 020503.

Thompson, J. D., Zwickl, B. M., Jayich, A. M., Marquardt, F., Girvin, S. M., and Harris, J. G. E. (2008, March). Strong dispersive coupling of a high-finesse cavity to a micromechanical membrane. *Nature*, **452**(7183), 72–5.

Treutlein, P., Chung, K. Y., and Chu, S. (2001, May). High-brightness atom source for atomic fountains. *Physical Review A*, **63**(5), 51401.

Treutlein, P., Genes, C., Hammerer, K., Poggio, M., and Rabl, P. (2014). Hybrid mechanical systems. In *Cavity-Optomechanics* (ed. M. Aspelmeyer, T. Kippenberg, and F. Marquardt), pp. 327–351. Springer-Verlag, Berlin.

Treutlein, P., Hunger, D., Camerer, S., Hänsch, T. W., and Reichel, J. (2007). Bose–Einstein condensate coupled to a nanomechanical resonator on an atom chip. *Phys. Rev. Lett.*, **99**, 140403.

Vasilakis, G., Shen, H., Jensen, K., Balabas, M., Salart, D., Chen, B., and Polzik, E. S. (2015, March). Generation of a squeezed state of an oscillator by stroboscopic back-action-evading measurement. *Nature Physics*, **11**(5), 389–92.

Vogell, B., Kampschulte, T., Rakher, M. T., Faber, A., Treutlein, P., Hammerer, K., and Zoller, P. (2015, April). Long distance coupling of a quantum mechanical oscillator to the internal states of an atomic ensemble. *New Journal of Physics*, **17**(4), 043044.

Vogell, B., Stannigel, K., Zoller, P., Hammerer, K., Rakher, M. T., Korppi, M., Jöckel, A., and Treutlein, P. (2013, February). Cavity-enhanced long-distance coupling of an atomic ensemble to a micromechanical membrane. *Physical Review A*, **87**(2), 023816.

Wang, Y.-J., Eardley, M., Knappe, S., Moreland, J., Hollberg, L., and Kitching, J. (2006, December). Magnetic resonance in an atomic vapor excited by a mechanical resonator. *Physical Review Letters*, **97**(22), 227602.

Weber, T. M., Höning, M., Niederprüm, T., Manthey, T., Thomas, O., Guarrera, V., Fleischhauer, M., Barontini, G., and Ott, H. (2015, January). Mesoscopic Rydberg-blockaded ensembles in the superatom regime and beyond. *Nature Physics*, **11**, 157.

Weidemüller, M. and Zimmermann, C. (eds.) (2009). *Cold Atoms and Molecules*. Wiley-VCH, Berlin.

Wilson, D. J., Regal, C. A., Papp, S. B., and Kimble, H. J. (2009, November). Cavity optomechanics with stoichiometric SiN films. *Physical Review Letters*, **103**(2), 207204.

Winoto, S. L., DePue, M. T., Bramall, N. E., and Weiss, D. S. (1999). Laser cooling at high density in deep far-detuned optical lattices. *Physical Review A*, **59**(1), 19–22.

Wolke, M., Klinner, J., Kessler, H., and Hemmerich, A. (2012, July). Cavity cooling below the recoil limit. *Science*, **337**(6090), 75–8.

Xuereb, A., Domokos, P., Horak, P., and Freegarde, T. (2010, September). Scattering theory of multilevel atoms interacting with arbitrary radiation fields. *Physica Scripta*, **T140**(T140), 014010.

Yeo, I., de Assis, P.-L., Gloppe, A., Dupont-Ferrier, E., Verlot, P., Malik, N. S., Dupuy, E., Claudon, J., Gérard, J.-M., Auffeves, A., Nogues, G., Seidelin, S., Poizat, J-Ph., Arcizet, O., and Richard, M. (2013, December). Strain-mediated coupling in a quantum dot–mechanical oscillator hybrid system. *Nature Nanotechnology*, **9**(2), 106–10.